Accepted Manuscript

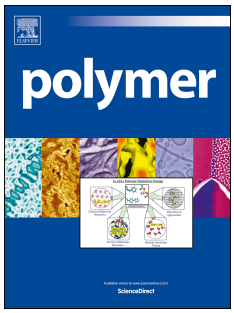

Thermally recyclable polylactic acid/cellulose nanocrystal films through reactive extrusion process

Prodyut Dhar, Debashis Tarafder, Amit Kumar, Vimal Katiyar

PII: S0032-3861(16)30084-2

DOI: 10.1016/j.polymer.2016.02.004

Reference: JPOL 18436

To appear in: *Polymer*

Received Date: 2 October 2015

Revised Date: 31 December 2015

Accepted Date: 2 February 2016

Please cite this article as: Dhar P, Tarafder D, Kumar A, Katiyar V, Thermally recyclable polylactic acid/cellulose nanocrystal films through reactive extrusion process, *Polymer* (2016), doi: 10.1016/j.polymer.2016.02.004.

Thermally Recyclable Polylactic Acid/Cellulose Nanocrystal Films Through Reactive Extrusion Process

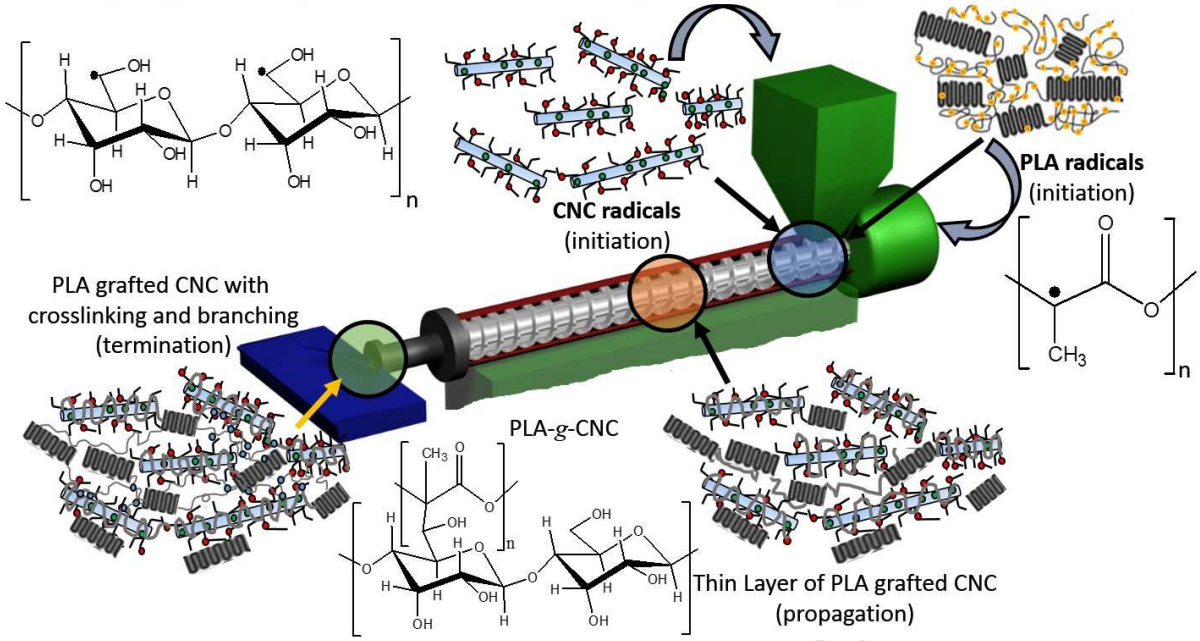

Thermally Recyclable Polylactic Acid/ Cellulose Nanocrystal Films Through Reactive Extrusion Process

*Prodyut Dhar, Debashis Tarafder, Amit Kumar and Vimal Katiyar**

Department of Chemical Engineering, Indian Institute of Technology Guwahati, Guwahati, 781039, Assam, India.

*Corresponding author, email: vkatiyar@iitg.ac.in

Abstract

This paper reports a single step reactive extrusion process for fabrication of thermally stable, polylactic acid grafted cellulose nanocrystal(PLA-*g*-CNC) nanocomposite films using dicumyl peroxide as crosslinking agent. PLA-*g*-CNC nanocomposites were recycled without significant breakage in the molecular structure of PLA. The grafted PLA chains shields the sulfate and hydroxyl groups of CNCs, thereby enhancing the compatibilization with PLA matrix and preventing thermal degradation during extrusion. NMR and FTIR spectroscopy studies showed that amorphous PLA chains grafted on CNC surface through C–C bonds formation. Presence of such chemical crosslinks led to efficient transfer of modulus of CNCs to PLA matrix, thereby improving the tensile strength and young's modulus by~40% and~490%,respectively. Recycling

of PLA-*g*-CNC doesn't alter the molecular weight, thermal, crystallization and mechanical properties of the nanocomposites significantly. Therefore, the current study provides a novel approach for fabricating CNC-reinforced-PLA nanocomposites which can be easily recycled and reused for multiple cycles.

Keywords: cellulose nanocrystal, polylactic acid, nanocomposites.

Introduction

Polylactic acid (PLA) is a bio-based thermoplastic polymer derived from renewable resources (e.g. corn, starch, sugarcane, etc.) which has the potential to replace the petroleum-derived polymers and solve the problems related to their sustainability. Among all the bio-based polymers, PLA has attracted considerable interest because of its easy processability and comparable mechanical and thermal properties in comparison to conventional synthetic polymers. However, the brittle nature, inferior oxygen or water vapor barrier properties and heat distortion temperature (~55ºC) [1] limits its application for manufacturing commodity products. Therefore, modifications of PLA through physical approaches like incorporation of nanofillers [2,3], plasticizers [4,5] and blending [6] as well as through chemical approaches like polymerization through different routes such as grafting onto and from approaches [7,8] have been extensively researched.

Cellulose nanocrystals (CNCs) are fabricated by extracting the crystalline segments of cellulose through controlled acid hydrolysis of feedstocks derived from renewable biomass resources. CNCs have relatively improved mechanical properties with high tensile strength and elastic modulus (~140–220 GPa) (compared to other high-strength materials such as glass fiber, Kevlar etc.,), which depends on the biomass feedstock and the acid system used for cellulose

hydrolysis [9]. The rod-like morphology of CNCs alongwith its high hydroxyl functionality and surface area makes it a strong reinforcing agent, that can form a percolated network-like structure in thermoplastics such as PLA [10]. Presence of such network imparts the desired and targeted properties of CNCs to the polymeric matrix. However, the effective dispersion of CNCs in the polymer matrix depends on the surface modification approaches and PLA processing methodology (solution casting or extrusion) employed. Surface modification of CNCs through strong oxidizing agents such as TEMPO (2,2,6,6-tetramethylpiperidin-1-yl)oxyl [11] or ammonium peroxidosulfate [12], immobilizing monomeric units [13], surface acetylation [14], silanization treatment [15], carboxylation-amidation reaction [16], plasticizers [17], adsorption of surfactants [18] etc. results in improved dispersion of CNCs in polymer matrix through solution casting process.

Processing of PLA/CNC nanocomposites through melt extrusion process is a challenging task as it leads to the agglomeration of hydrophilic CNCs in PLA matrix due to the presence of strong intermolecular hydrogen bonding [19]. PLA is susceptible to thermal degradation during melt extrusion which leads to the reduction in bulk properties such as mechanical, gas barrier, thermo-physical properties. CNCs self-assemble to form non-dispersible agglomerates (under freeze or air drying conditions) in dry state [20] and the sulfate groups of CNC surface (acquired during sulphuric acid hydrolysis) act as catalyzing agent for the degradation of both CNCs and PLA during extrusion [21]. To overcome such challenges researchers have used two different approaches: firstly, hydrophilic polymers are adsorbed on CNC surface (using physical or chemical methods) to mask the sulfate groups [22], and secondly, reactive extrusion is carried out in the presence of chain extenders [23]; such studies however are scarce. Also, to the best of

our knowledge, studies reporting recycling of polymer-CNC nanocomposites (without altering the polymeric properties significantly) hasn't been reported in the literature till date.

Recently, several studies have been reported on reactive extrusion of PLA in the presence of various chain extenders and radical initiators which lead to improvement in melt strengthening thereby widening the processing window of PLA. Marsilla & Verbeek [25] grafted itaconic anhydride on PLA through radical grafting process, which led to improvement in the tensile strength and elongation at break (~60 %). Spinella et al. [26] developed a green approach using titanium tetrabutoxide for reactive blending of PLA with poly (ω-hydroxytetradecanoic acid) compatibilizing through trans-esterification reaction. This led to significant improvement in the elongation at break (by ~140%) and impact strength (by ~2.4 times). Interestingly, it was found that reactive extrusion based PLA composites retained the inherent biodegradable nature and were readily compostable and degradable under hydrolysis conditions [24] . Similarly, *in situ* compatibilization of PLA with poly (butylene adipate-co-terephthalate) lead to improvement in the impact toughness and elongation at break (by ~300%) [24]. Yang et al. [28] achieved significant increase in thermal stability of PLA by incorporating trace amount of crosslinking agent. Blending of PLA with poly (3-hydoxybutyrate-co-4- hydroxybutyrate) in the presence of dicumyl peroxide (DCP) initiator resulted in high crosslinking which showed typical toughening with improvement in tensile strength [25]. Grafting of maleic anhydride in the presence of an initiator showed slight increase in molecular weight of PLA, possibly due to crosslinking or increase in chain entanglements [26]. Recent studies on the effect of radical initiators on the rheological properties of PLA confirms that the increase of branching leads to improvement in the melt strength by approximately three times with higher shear sensitivity [27],[28],[29]. However, studies on reactive extrusion of polymers in presence of fillers or nanofillers have been

rarely reported. Wang et al. [34] grafted bamboo flour onto PLA using benzoyl peroxide and *tert*-butyl peroxy benzoate (as initiators) and glycidyl methacrylate (as chain extender). Improved compatibility between the two phases was observed which led to enhancement in the mechanical strength and modulus by 44 and 135% respectively, along with increase in the thermal properties. Recent studies [30] on *in situ* reactive extrusion of PHB with cellulose in the presence of DCP led to improvement in the glass transition temperature and onset degradation temperature (by ~22ºC), along with significant decrease in the crystallinity.

In the present work, PLA is grafted on CNCs through reactive extrusion process in the presence of DCP (as radical initiator) and the effect on the mechanical, thermal and crystallization properties are extensively studied. The grafting is confirmed through fourier transform infrared spectroscopy (FTIR) and the possible mechanism is explained from nuclear magnetic resonance (NMR) analysis. X-ray Diffraction (XRD) and differential scanning calorimetry (DSC) studies are carried out to understand the effect of grafting parameters on the change in crystallinity of PLA. The effect of grafted CNCs on the mechanical properties of the nanocomposites is investigated with dynamic mechanical analyzer (DMA) and tensile studies. We report for first time an industrially viable, thermally reprocessible process for the fabrication of PLA/CNC nanocomposites which could be recycled without any significant change in the PLA properties.

Experimental Section

Materials. Poly L-lactic Acid (PLA) (grade: 4032D, L-lactic acid/D-lactic acid: 98.6/1.4) used in this study was supplied by Nature Works® LLC., USA. The weight average (M_w) and number average molecular weight (M_n) of PLA 4032 were obtained using Gel Permeation Chromatography (GPC) (calibrated with polystyrene standards) and found as ~200,000 and

~150,000 Da respectively. Bamboo pulp received from Hindustan Paper Corporation Limited (HPCL, Nagaon, India) was pretreated by soda pulping method followed by bleaching to extract the purified cellulose. Sodium hydroxide (>97%), sodium hypochlorite (4%), hydrogen peroxide (30%) and sulphuric acid (>99%) (Analytical grade) used for the CNC fabrication were purchased from SISCO Research laboratories (SRL Chemicals, India). Dicumyl Peroxide (DCP), used for reactive extrusion as radical initiator, was purchased from Sigma Aldrich, India. Chloroform (Merck, HPLC grade) and deutrated chloroform (Merck, India) was used as received for the GPC and NMR measurements.

Fabrication of Cellulose Nanocrystals

Bamboo pulp was pretreated through soda pulping method (2 wt% sodium hydroxide at 80ºC for 2 hours) followed by bleaching (2 wt% hydrogen peroxide and sodium hypochlorite treatment at 80°C for 2 hours) to remove the hemicellulose and lignin impurities. Acid hydrolysis of the purified pulp (1.0 g) was carried out with sulphuric acid (64 wt%) as previously reported [31],[32]. The hydrolysis reaction was stopped by adding chilled deionized water followed by centrifugation (~10,000 rpm) to remove the excess acid. The CNC suspension was dialyzed with distilled water using cellulose acetate membrane (cut off molecular weight ~14,000 Da, Sigma Aldrich) until a final pH of ~7 was attained. Subsequently, the final suspension was lyophilized for 24 hours at –30 °C to obtain the freeze dried CNCs.

Reactive Extrusion of PLA-*g*-CNC Nanocomposites

PLA granules and freeze dried CNCs were vacuum dried at 40ºC overnight to remove the adsorbed moisture. DCP, the radical initiator (1.2 wt. %) used in this study, was dissolved in acetone (10 ml) and sprayed on PLA beads. The PLA beads were further dried in vacuum at 40ºC to remove the excess acetone before processing. The DCP coated PLA granules (10 g) were

mixed with CNC (at different ratios 1–3wt. %) in a beaker and extruded in a twin screw extruder (Haake Rheomix). The extrusion parameters, i.e. screw speed and processing temperature were maintained at 50 rpm and 180°C respectively with a recycle time of 5 minutes. The PLA-*g*-CNC nanocomposites were extruded into strips of dimension ~ 5mm (width) × 0.5mm (thickness). Hereafter, the PLA-*g*-CNC nanocomposites extruded in the presence of DCP and with various loadings of CNCs (1–3wt. %) are represented as PLAD, PLADCNC1, PLADCNC2 and PLADCNC3, respectively.

The extruded strips (in the presence of DCP) were washed in excess chloroform for 24 hours to remove the unreacted DCP and non-grafted PLA. The suspension was vacuum filtered (filter paper of pore size ~ 450μm) and the grafted PLA/CNC gel was washed with excess chloroform to remove the ungrafted PLA several times and the gel left over after filtration was collected. The gel was dried in vacuum (~50°C) to remove the trapped chloroform and the gel yield (%) was calculated using equation (1).

$$gel\ \% = \frac{W_{gel}}{W_i} \times\ 100 \quad (1)$$

where W_{gel} and W_i are the mass of dry gel after vacuum drying and initial mass of extruded strips before dissolving in chloroform, respectively.

Several other grafting parameters such as graft percentage (%GP), grafting efficiency (%GE) and weight conversion (%WC) were also calculated as reported in the literature [30]. Graft percentage represents the mass of the grafted PLA with respect to initial mass of CNCs, as defined in equation (2).

$$\%GP = \frac{(W_{gel} - W_{CNC})}{W_{CNC}} \times 100 \quad (2)$$

Graft efficiency (GE), measures the mass of PLA grafted onto the CNCs and is represented as in equation (3).

$$\%GE = \frac{(W_{gel} - W_{CNC})}{W_{PLA}} \times 100 \quad (3)$$

Weight conversion (WC) measures the percentage of the CNC grafted and is defined in equation (4).

$$\%WC = \frac{W_{gel}}{W_{PLA}} \times 100 \quad (4)$$

where W_{gel}, W_{PLA} and W_{CNC} represent the mass of grafted PLA/CNC gels, PLA and CNC respectively.

After washing the PLA-*g*-CNC nanocomposites with chloroform to remove the ungrafted PLA chains, the change in the wt. % of the CNC in the reprocessed PLA-*g*-CNC (rPLACNC) nanocomposites are calculated using the following equation (5):

$$\%\text{CNC in rPLACNC nanocomposites} = \frac{W_{CNC}}{W_{gel}} \text{ x } 100 = \frac{GE}{GP} \times \frac{100}{WC} \times 100 \quad (5)$$

Reprocessing of the PLA-*g*-CNC grafted gels

The vacuum dried PLA-*g*-CNC gels were chopped into small strips and were further reprocessed through the extruder for all CNC weight fractions. The parameters for extrusion were kept similar to the first processing, i.e. screw speed at 50 rpm, extrusion temperature of 180°C and recycle time of 5 min. The dimension and drawing speed of the extruded strips were also kept constant. Hereafter, the reprocessed PLA-*g*-CNC samples for all weight percent of CNCs (1–3wt. %) are represented as rPLA, rPLACNC1(1.35), rPLACNC2(3.33) and rPLACNC3(5.15) with the numbers in bracket representing the probable CNC wt. % present in the samples after the ungrafted PLA have been removed (calculated using eq. (5)).

Analytical Instrumentation and Characterization.

Powder X-ray Diffraction (XRD). The wide angle X-ray diffraction (WAXD) studies were carried out with D8 Advance diffractometer (Bruker, Germany) equipped with Cu-K_α radiation

(λ= 0.1541 nm) as X-ray source operating (40 kV, 40 mA) at scan rate of 0.05° per 0.5 s in the 2θ range 10–50°. The crystallite size of PLA and reactively extruded PLA-*g*-CNC nanocomposites was determined using the Diffractogram v2.0 software.

*Fourier Transform Infrared Spectroscopy (FTIR).*The chemical grafting studies of PLA-*g*-CNC nanocomposites were conducted in transmission mode using Perkin Elmer (Frontier) spectrometer, in attenuated total reflection (ATR) mode using ZnSe crystal in the range of 4000–500 cm^{-1} with resolution of 4cm^{-1} for 128 scans.

Field Emission Scanning Electron Microscope (FESEM). The extruded strips were placed on a stub with carbon tape and coated with gold in sputtering unit for 180s. To study the fracture behavior of PLA-*g*-CNC films, the samples after tensile studies were immediately immersed into liquid nitrogen. Thereafter, surface morphology of the samples were examined using FESEM (ZEISS, USA) at an accelerating voltage of 2-5kV.

Gel Permeation Chromatography (GPC). The molecular weight of the extruded samples were determined using high performance liquid chromatography (HPLC), Shimadzu LC-20A system (Shimadzu, Japan) equipped with two PLgel 5μm mixed D columns (Agilent, UK) in series which were calibrated using polystyrene standards in chloroform. The extruded samples (~20mg) were dissolved in HPLC grade chloroform for 3 days and filtered with 0.2μm filter paper before analysis. The measured molecular weight distribution (MWD) for the cross-linked/ branched PLA is not exact because of the change in the hydrodynamic volume; however, significant amount of information could be obtained from this study.

Differential Scanning Calorimetry (DSC). The thermal properties of the PLA and reactively extruded PLA/CNC samples were characterized with Netzsch DSC (Germany) under inert nitrogen gas flow (~60ml/min). DSC studies were carried out at a scanning rate of 10°C/min

with temperature varied from 25°C to 190°C for both heating and cooling cycles. The calibration was carried out using Indium standard beforehand and samples weighing ~5-6 mg were placed on a platinum crucible for analysis.

Universal Testing Machine (UTM). The mechanical studies of the extruded samples (specimen size: 50mm x 5 mm (length x width)) were carried out following the standard protocol ASTMD 882, with the universal testing machine (UTM) (Kalpak Instruments, India) equipped with a load cell of 500N at a constant speed of 10mm/min.

Optical Polarimetry. The specific and optical rotation of the PLA and PLA-*g*-CNC samples (20 mg dissolved in 20ml chloroform) were measured with AUTOPOL II (Rudolph Research Laboratory, USA) at a wavelength of 589 nm using self-calibrated mechanism.

Nuclear Magnetic Resonance (NMR). The chemical structures of PLA and PLA/CNC gels were studied with 600MHz nuclear magnetic resonance (NMR) spectrometer (Bruker, Germany). The samples were dissolved in deutrated chloroform ($CDCl_3$) for 3 days and filtered with 0.25 µm filter (3 times) before analysis.

Dynamic Mechanical Analyzer (DMA). The thermo-mechanical analysis of the extruded strips was carried out with DMA242 (Netzsch, Germany) in tensile mode under a dynamic force of 2 N, amplitude of 20µm at a frequency of 1 Hz. Samples were cut into 5 mm x 5 mm x 0.5 mm strips and measurements were carried out in the temperature range of 25-90°C at a heating rate of 2°C/min.

Results and Discussion

In situ reactive grafting of PLA on CNC: Reaction mechanism, grafting parameters and molecular weight studies.

Reactive grafting of PLA on CNC (PLA-*g*-CNC) surface was successfully carried out through extrusion process in presence of DCP which decomposes into free radicals at high temperature. The activity of the DCP initiated peroxide radicals (as shown in Scheme 1a) is short (~180s) [33],[34], due to which grafting reaction took place during the initial 5 minutes of the extrusion process under high shear conditions. To achieve effective grafting, optimization of the reactive extrusion process in terms of parameters such as screw speed, temperature and DCP content was carried out. It was found that a screw speed of 50 rpm, extrusion temperature of 180ºC, and DCP content of 1.2% was effective in achieving high molecular weight (data not shown). A residence time of about 5 min was selected because of the short life of DCP radicals as well as previous studies also report maximum gel yield under similar conditions [30]. At such optimized conditions, the effect of different CNC loadings (1–3 wt %) on grafting parameters and properties of PLA fabricated through extrusion process were investigated in detail. During the reactive extrusion process, it was found that the complex viscosities of these samples (~50-70 Pa.s at various CNC loadings) were higher in comparison to neat PLA (~40 Pa.s), probably due to the formation of branched and cross-linked structures [35].The PLA-*g*-CNC formed micro gel-like structure which was filtered out and extracted in chloroform, to remove the unreacted PLA. It was found that the incorporation of CNCs into PLA during reactive extrusion process enhances the formation of gel and grafting percentage. Table 1 summarizes the effect of CNC loading on the percentage gel yield, graft percentage, graft efficiency, weight conversion, specific rotation and optical rotation respectively during the reactive extrusion process. The maximum grafting efficiency and gel yield % was found to be 40.7 and 76.8 % respectively for PLADCNC1 (Table 1). Gel yield decreases at higher CNC loadings, probably due to thermally induced chain scission during extrusion, catalyzed by the high content of sulfate groups present

on CNC surface which suppress the grafting reaction. Moreover, the agglomeration of CNCs at higher loadings decreases the number of available $-CH_2OH$ groups on CNC surface for the grafting reaction to take place. The specific and optical rotation of PLA-*g*-CNC changes compared to neat PLA, by ~21º and 0.1º respectively. This is possibly due to the grafting of CNCs on the chiral center carbon of PLA which hindered the specific rotation [36].

To confirm the grafting of PLA on the CNC surface, chemical structure analyses were carried out through FTIR and NMR spectroscopy. PLA showed characteristic FTIR peaks at 1748, 1180, 1128, 1078, 1042, 868 and 954 cm^{-1} corresponding to C=O stretching, C–O–C asymmetric stretching, C–OH side group vibrations, C–C vibrations and –CH stretching [37](Figure 1). CNC showed characteristic FTIR peaks at 3402, 2908, 1647, 1427, 1319, 1203, 1163,1031 and 896 cm^{-1} corresponding to –OH stretching, -CH stretching, -OH bending, $-CH_2$ bending, - CH_2 wagging, C-OH bending in plane at C-6, -C-O-C asymmetric stretching of β-glucosidic linkage, C-OH stretching in plane at C-6 and -C-O-C asymmetric bending of β-glucosidic linkage respectively[10]. The FTIR peaks at 2854, 2924 and 1380 cm^{-1}, corresponding to the symmetric, asymmetric stretching and deformation of $–CH_3$ groups, were present in all the samples. (Figure 1(b)). The peak at 1180 cm^{-1} corresponding to C–O–C stretching, were present in PLA Neat, PLAD and rPLACNC1(1.35) (with decreased in intensity compared to pristine PLA due to grafting), however, it shifted to 1164 cm^{-1} in case of PLADCNC1. The peak at ~1128 cm^{-1} corresponding to CH_3 rocking, is visible for the PLA Neat, however, slight shift in peaks were found for PLAD to ~1124 cm^{-1}, for rPLACNC1(1.35) to ~ 1122cm^{-1} and PLADCNC1 to ˜1122 cm^{-1}. Similarly ,the peak at ~1454 cm^{-1} corresponding to CH_3 vibration asymmetric bending for neat PLA and PLACNC1, shifted to ~1464cm^{-1} for the PLA-*g*-CNC gels and reprocessed rPLACNC samples. The shift in peaks of C–O–C stretching , $–CH_3$ rocking and bending is probably due to the grafting of

PLA with CNCs alongwith the formation of high molecular weight cross-linked PLA-*g*-CNC branched nanocomposites [30]. The peaks at 2998 and 1362 cm^{-1} present in PLA and PLACNC1, corresponding to the –CH vibration and stretching respectively, were significantly diminished in all the extruded samples (in the presence of DCP) (Figure 1(b) & (d)). In the case of the PLADCNC1 and rPLACNC1, the –CH stretching peak of PLA at 1042 cm^{-1} was absent and a new peak at 1020 cm^{-1} corresponding to formation of new C–C linkage due to grafting between the PLA and CNCs was found. CNCs show their characteristic peaks at 1028 and 1203cm^{-1} for the C-OH stretching and bending in plane at C-6 which were found to be present in the PLA-*g*-CNC gels and reprocessed samples, however, slightly shifted to 1020 and 1208 cm^{-1} respectively. Presence of such peaks confirms the formation of the grafting between the C(6)-OH of the CNCs with the methine groups of PLA (as shown in Scheme 1).Moreover, the carbonyl peak for pristine PLA shifted from 1748 cm^{-1} to 1740 cm^{-1} during extrusion (in presence of DCP only) (Figure 1(c)), due to the grafting of $–CH_2OH$ groups in CNCs onto the methine groups of PLA. ^{1}H NMR spectroscopy analysis of PLA-*g*-CNC samples (PLADCNC1) also showed new characteristic peaks at 3.68 ppm and in the 4.1–4.5 ppm range[38] (see Figure 2) which confirms the grafting. The new peak at 3.68 ppm corresponds to the methine protons formed in the PLA-*g*-CNC structure (marked as 'a' in the inset of Figure 1(e)). Presence of such methine protons was also reported in case of PLA grafted maleic anhydride based wood flour composites and PLA grafted with polyethylene glycol systems in presence of DCP (~3.6 ppm)[39] [40]. The peaks in the range of 4.1–4.5 ppm correspond to the methylene protons of the cellulose backbone, which confirms the presence of CNCs in the grafted structure [42]. In the ^{1}H NMR spectra of pristine PLA (Figure S1), the peak at 3.68 ppm was found to be absent and the peaks at 5.19 and 1.46 ppm which represent the CH and CH_3 protons, were found to have no significant

shift/changes in comparison to ^{1}H NMR spectra of PLA-*g*-CNC. The grafting efficiency was calculated for PLA-*g*-CNC under various CNC loadings (1–3 wt %) by integrating the peak area at 3.68 ppm. It was found that the grafting efficiency was highest in the case of 1 wt% CNC loading and decreased with increase in CNC loading, consistent with the calculations for gel yield (from equation (1)) as shown in Table 1. The peroxide radicals generated at high temperature react with both PLA and CNC under high shear conditions, abstracting hydrogen from both leading to the formation of stable micro radical structures (Scheme 1b). These radicals are highly reactive and diffuses effectively in molten PLA (during extrusion) thus generating higher concentrations of these radicals in the PLA phase. Due to the impermeable crystalline nature of CNC, the generated PLA radicals (containing DCP) could only react with surface –CH_2OH groups of CNCs forming a thin overlapping layer of PLA surrounding the CNCs (Scheme 1c). Formation of such thin layer of PLA chains, grafted onto the CNC surface, through this radical approach is an instantaneous process and provides better interfacial compatibility between PLA and CNC. The FTIR peaks of PLA-*g*-CNC samples (see Figure 1(d)) showed that peaks corresponding to the amorphous segments of PLA at 1265 and 955 cm^{-1} disappeared while the low intensity peak at 1210 cm^{-1}, corresponding to crystalline segments of PLA [41], remained. The amorphous chains of PLA which are randomly entangled (in the molten state) on grafting with the CNCs organized into ordered positions along the surface of nanocrystals (which are highly ordered stacks of cellulose chains). This preferentially led to the orientation of the amorphous segments of PLA chains into possible ordered state or crystalline orientation along the surface of CNCs which resulted in increase in the crystalline nature of PLA-*g*-CNC nanocomposites as explained from XRD and DSC studies subsequently. Further, as the reaction propagates under high shear mixing conditions, two different mechanisms could probably occur

313 in the extruder. Firstly, the radicals generated in PLA could further diffuse in the crystalline
314 domains of CNCs forming a PLA-engulfed-CNC network-like structure which acts as a
315 compatibilizer for uniform dispersion of CNC into the PLA matrix during the melt blending
316 process. Presence of such chemically grafted PLA chains on CNCs leads to enhanced
317 compatibility and avoids irreversible agglomeration of hydrophilic CNCs during extrusion with
318 hydrophobic PLA. Secondly, the PLA radicals could crosslink among each other (termination by
319 combination) forming a branched chain-like structure growing on the PLA-*g*-CNC structures
320 (Scheme 1c). Moreover, the presence of such PLA wrapped CNCs leads to shielding of the
321 surface sulphate groups of CNCs, preventing the black coloration typically observed in CNC
322 based composites when extruded using traditional approaches (discussed in subsequent section).
323 Figures 2(a) & (b) show the weight average (M_w) and number average (M_n) molecular weight
324 distribution (MWD) and polydispersity index (PDI) of reactively extruded PLA/CNC films at
325 different CNC loadings. Reactive extrusion of PLA with DCP in the presence of CNC (1–3 wt%
326 range) shows an increase in both M_w and M_n by ~40 %. Such drastic increase in MWD is
327 however absent during reactive extrusion of PLA in the presence of DCP alone. The PDI of the
328 PLA-*g*-CNC did not changed significantly and was found to be ~ 2, which suggests that the
329 chain length of branched PLA were formed with uniform distribution even at different CNC
330 loadings. The GPC chromatograms (Figure S2) for PLA-*g*-CNC were broader compared to those
331 for PLA and show the presence of two small distinct shoulders both at high and low molecular
332 weight regions. This can be attributed to two possible phenomenon occurring during the reactive
333 extrusion process: chain extension in the presence of DCP (leading to chromatogram shift to
334 high MWD region) and chain scission in the presence of CNCs (leading to shift to low MWD
335 region). In the former case, as shown in Figure S2, the molecular weight corresponding to

shoulder peak in PLA-*g*-CNC was found at least two times higher than neat PLA. This indicates that the PLA chains cross-linked to form a tree-like or more complex branched structure [42]. The area of the high molecular weight peak (retention time ~ 11 min) increased and formed small shoulder for PLADCNC1 (~88%) and PLADCNC2 (~90%) in comparison to the neat PLA (~78%). The increase in MWD in the presence of CNCs is due to the presence of $–CH_2OH$ groups in CNC which act as active sites for the generation of radicals, which leads to the propagation and growth of the PLA chains on CNC surface (as discussed in Scheme 1(b) & (c)). However, on increasing the CNC loading (~3 wt %), the area of the high molecular weight peak decreased (~70%) and that of the low molecular weight peaks (at retention time ~ 16.4 and 17.2 min) increased (~12 and 16% respectively). This is probably due to the presence of high concentration of sulfate groups or agglomeration of CNCs (at higher loadings), which interfere during reactive extrusion process thereby degrading the PLA at higher processing temperatures. It is noteworthy to mention that the area of low molecular weight fractions (at retention time ~16.7 and 17.3 min) for PLADCNC1 (~1.7 and ~10.3% respectively) and PLADCNC2 (~4 and 5% respectively) decreased compared to neat PLA (~8.4 and ~13% respectively) (Figure S3). This is probably because grafting of PLA chains on the - CH_2OH groups of CNC moieties shields the sulfate and hydroxyl groups which are responsible for chain scission and alongwith it DCP acts as cross-linking agent which led to the increase in the molecular weight of the PLA chains due to propagation reaction (Scheme 1). Also, on comparing the GPC chromatograms of the NPLA and PLAD, it is found that reactive processing in presence of DCP helps in preventing the thermal induced degradation of PLA during extrusion process significantly. However, at higher CNC loadings (~3 wt. %) the grafting efficiency decreased due to agglomeration of CNCs, which subsequently leads to the degradation of PLA during extrusion.

Effect of reprocessing of the PLA-grafted-CNC gels on structure and molecular weight.

Extracted PLA-*g*-CNC gel was vacuum dried and subsequently extruded into strands using process conditions detailed in the experimental section. The FTIR and NMR spectra of the reactively extruded and reprocessed PLA-*g*-CNC composites did not show any significant difference in chemical structure (see Figure 1 and Figure S1 (b)), which is due to the presence of C–C bonds that are stable enough during reprocessing. GPC studies showed that recycling of the PLA-*g*-CNC gel led to decrease in M_w and M_n by ~18 and 15% only (at~3wt % loading) (Figure 2(a)), which is less compared to traditional PLA/CNC extrusion (~22 and 18% at 1wt. % CNC loadings during first time extrusion). The reactive extrusion based grafting approach effectively masks the interaction of sulfate and hydroxyl groups in CNCs with PLA, thereby preventing the drastic reduction in molecular weight. The PDI was found to be ~1.8 for recycled samples, which was lower than that of PLA-*g*-CNC probably due to chain scission of the long branched PLA chains during extrusion. However, after reprocessing the GPC chromatogram was found to be sharper, with a decrease in the shoulder area for high molecular weight peak and increase in number of peaks in the low molecular weight region. The area of the high molecular weight shoulder peak decreased from ~89 to 68% for 1 and 3 wt% CNC loadings respectively. Moreover, three low molecular weight peaks were found (at retention time ~16.5, 17.3 and 17.6 min), whose area increased with the higher CNC loadings (~8.46, 6.4 and 6.1% respectively at 3 wt% CNC loading) (Figure S2). This is possibly due to lower grafting efficiencies at ~3 wt% CNC loadings, which enhances the thermal degradation of PLA due to presence of sulfate and hydroxyl groups. However, the decrease in MWD is not significant enough compared to the traditional approach of PLA/CNC processing and recycled polymers with M_w ~ 250 kDa finds potential engineering applications.

Morphological studies

Figure 4(a) compares the physical appearance of the reactively extruded PLA, PLADCNC1 and rPLACNC1(1.35) with the PLA/CNC 1 wt% extruded by simple melt blending at similar processing conditions. Extrusion of the freeze dried CNCs with pristine PLA showed the formation of black agglomerated particles, which is probably due to the degradation of the sulfate groups in CNCs at high shear and temperature. Moreover, the FESEM micrograph for the PLA/CNC1 nanocomposite processed through traditional approach showed the presence of large agglomerations of the freeze dried CNCs (marked in square box Figure 4b). However, the reactive extruded PLA-*g*-CNC strips were transparent and didn't produced such black agglomerated particles during extrusion, at all CNC loadings. Even the recycled strips were found to be stable and transparent. As explained earlier, the reactive extrusion being an instantaneous process, the radicals generated on CNCs surface reacts with PLA chains thereby shielding the sulphate groups which are responsible for degradation during extrusion process. Moreover, the presence of such PLA encapsulated CNC showed better interfacial compatibility with the PLA matrix which led to improved dispersion (as shown in Figure 4(c) & (d)). Figure 4(c), shows the presence of micro-gel like domains of branched PLA- *g*- CNC (in square box) alongwith the rod-like CNCs which are uniformly distributed in the matrix. Magnified micrograph of the circular region (inset Figure 4(c) at ~20KX) shows the presence of smooth interphase between the micro-gel domains of PLA matrix with CNCs. The CNCs fabricated through sulphuric acid hydrolysis were 700±50nm in length and 30±8nm in width (Figure S4). However, the dimensions of the PLA-*g*-CNCs after reactive extrusion changed significantly with increased length of 1.5±.3µm and diameter of 120±8nm. The increase in the dimensions is probably due to the presence of grafting between the hydrophilic CNCs with the hydrophobic

PLA through reactive extrusion in presence of DCP. Re-extrusion of the extracted PLA-*g*-CNC gel, shows smooth PLA matrix with absence of the micro-gel domains in the interphase (Figure 4d). The freeze dried CNCs (marked in black arrows) are randomly distributed without any phase separation. It suggests that the grafted CNCs even after reprocessing were stable and unaltered, which suggests its enhanced compatibility and dispersion in PLA matrix.

Thermal properties

Thermal degradation behavior of PLA-*g*-CNCs before and after recycling were investigated to predict the onset degradation temperature (T_{onset}), temperatures at which 10 and 50% reduction occur ($T_{10\%}$ and $T_{1/2}$) and % reduction weight at 300ºC. PLA showed a single step degradation profile, with a T_{onset} of ~306 ºC and $T_{1/2}$ of 356ºC which is due to hydrolysis and oxidative chain scission of PLA chains (Figure 5) [22]. In our previous studies [10], simple dispersion of CNCs into PLA matrix didn't showed any improvement in the thermal properties. The PLACNC1 nanocomposite prepared through traditional approach showed a slight decrement in $T_{1/2}$ ~1-2°C compared to neat PLA. However, grafting CNCs onto PLA in presence of small amount of DCP through reactive extrusion approach led to improvement in thermal stability of PLA. The T_{onset} and $T_{1/2}$ of PLADCNC1 was found to be improved by ~12ºC and ~5ºC respectively, compared to neat PLA (Figure 5). The percentage reduction in weight during the initial processing (upto ~300ºC) was also reduced significantly (only ~1.9 wt %) compared to traditional process. This is due to the formation of PLA encapsulated CNCs initially during reactive extrusion, which masks the sulfate and hydroxyl groups of CNCs, thereby delaying the degradation process. Also, the formation of C–C bond between the PLA and CNCs leads to enhanced thermal stability as higher activation energy is required to break such bridged linkages. Reprocessing the PLA-*g*-CNC nanocomposites led to the formation of low molecular weight fractions due to chain scission

under thermal stress conditions. This led to a decrease in the T_{onset} and $T_{1/2}$ of rPLACNC1(1.35), by 24ºC and 8ºC respectively, along with a reduction of ~5 % weight at 300ºC in comparison to PLADCNC1. Moreover, the reprocessed (rPLACNC1 (1.35)) sample, showed a weight loss ~4% at a temperature ~150°C, which is probably due to the presence of the of low molecular weight PLA chains as evident from the GPC chromatograms with peaks at retention time 16.7 and 17.4 min(~13.4 and ~17.5% area of GPC chromatograms respectively) (Figure S2) . In comparison to the other PLA-*g*-CNC nanocomposites (Figure 5), rPLACNC(1.35) have the highest fractions of the low molecular weight PLA chains(~ 30% area of the GPC chromatogram), hence it showed a significant weight loss at~150°C. Presence of such low molecular weight fractions is probably due to the chain scissions during thermal based recycling of PLA-*g*-CNCs in the extruder, which subsequently leads to decrement in the thermal properties. As shown in the inset of Figure 5, the reprocessed rPLACNC1(1.35) has almost similar degradation profile in the temperature range of 345–375ºC. Therefore, it can be concluded that the thermal properties of the PLA-*g*-CNC films do not alter significantly on reprocessing which is desirable for product fabrication.

Crystallization studies

XRD and DSC studies were carried out to understand the effect of both grafting and branching in PLA-*g*-CNC nanocomposites on their crystal structures. XRD diffractogram for the neat PLA showed representative peaks at 16.4º and 18.8º (see Figure 6), which correspond to the α-form of the PLA crystal with (010) and (110/200) planes [14]. Incorporation of the CNCs by grafting with PLA led to an increase in the intensity of the diffraction peak at ~16.4º, which suggests enhancement in the crystallinity of PLA. As explained in the previous section, this is probably due to the formation of C–C bonds between the PLA chains and the crystalline CNCs. Presence of such interaction probably leads to ordered arrangement of the amorphous PLA chains on the

CNC surface, which subsequently enhances the crystallinity of the nanocomposites. Similar observation of increase in crystallinity of the PLA based cellulose composites, due to uniformly dispersed cellulose microcrystal which in turn led to ordered arrangement of the PLA chains was reported by Lin et al. 2011[43] and Mukherjee et al. 2013[14]. The grafting was further confirmed by increase in d-spacing corresponding to the shift of peak 2Θ =18.8º for neat PLA to a lower 2Θ value of 18.3º for PLA-*g*-CNC (2 wt %) nanocomposites. Similar phenomenon of shift in 2Θ values to lower angles was also observed by Choi et al. [39], which suggests possible intercalation of CNCs into the PLA crystal structure during reactive grafting. The presence of CNCs in PLA-*g*-CNC films is confirmed from the low intensity peak at 2Θ=22.6º, corresponding to cellulose I crystal structure [10]. It might be due to the presence of high molecular weight PLA chains grafted onto the CNC surface, that the intensity of peak at ~22.6°, is not very sharp in case of the PLA-g-CNC nanocomposites. The XRD diffractograms do not change significantly for the reprocessed rPLACNC films, which suggests that the crystal structure does not change significantly after recycling.

DSC studies were carried out to understand the effect of heating and cooling cycles on the crystallization dynamics of reactively grafted PLA/CNC nanocomposites, as shown in Figure 7; the corresponding thermal parameters are listed in Table 2. The glass transition temperature (T_g) of PLA was found to be ~61.6ºC. On grafting CNCs reactively with PLA, the change in T_g was not significant (from second heating cycle) in comparison to neat PLA, probably because grafting restricted the motion of PLA chains. PLA grafted CNCs have shown lower T_g (first heating cycle) in comparison to neat PLA; which was suppressed with increase of CNC loading. This is probably due to the presence of ungrafted PLA chains or grafting of small PLA chains onto CNCs which have enhanced mobility thereby decreasing the T_g. Moreover, presence of

branching leads to formation of inter-spacing between the PLA chains, which undergoes shrinkage during first heating cycle thereby increasing chain mobility and decreasing T_g [44]. The specific heat (C_p) values corresponding to the change in the slope of T_g thermograms is determined through peak integration for all the PLA-*g*-CNC samples. Subsequently, the percentage of PLA chains that are grafted onto CNCs (% g-PLA) are calculated from the ratio of the C_p values for corresponding PLA-*g*-CNC samples to the C_p value of the neat PLA (Table 2). PLADCNC1 has the highest *g*-PLA value of 66%, which is in-line with its graft efficiency and gel yield of 40.7 and 74.2% respectively. It was found that on increasing the CNC loading, both the grafting efficiency (calculated from gel fraction) and *g*-PLA (calculated from DSC) decreases. It is noteworthy to mention that such approaches for determining the weight percentage of polymers grafted on CNCs have been reported elsewhere [30][45]. The decrease in *g*-PLA is probably due to the agglomeration of CNCs at higher loadings, which reduces the effective -CH_2OH groups available for grafting of PLA chains. We can vary the grafting length of PLA chains on the CNC surface by tuning the reactive extrusion process conditions, which in turn can result in significant change in polymer properties.

Figure 7 (a) and (b) shows the DSC thermograms for the first cooling and second heating cycles of reactively extruded PLA-*g*-CNC films. In the cooling cycle, neat PLA does not show any exothermic peak corresponding to the crystallization process. However, on reactive grafting of CNCs, sharp intense peaks corresponding to crystallization can be seen during the cooling cycle. This is due to the grafting of amorphous PLA segments on the CNCs through C–C crosslinks, which act as nucleating sites for crystal growth. The crystallization peak for PLAD occurs at 127.3ºC which decreases to 124.3ºC with increase in the CNC concentration (~3 wt. %). At higher CNC loadings, the % gel yield decreases and only 50% of PLA chains are grafted

497 onto CNC surface; therefore, the ungrafted chains undergo rearrangement to overcome the
498 energy barrier to form crystals at lower temperature. Formation of sharper crystallization peaks
499 along with higher ΔH_c values (~29 J/g) with increased CNC loadings (~3 wt%) also suggest that
500 higher fractions of ungrafted PLA chains have rearranged to form crystals [44]. The crystallinity
501 (X_c) of extruded PLA films is found to be ~28%. With incorporation of 2 wt% CNCs, the %
502 crystallinity (X_c) values increased slightly, because of the formation of C–C grafted sites with the
503 amorphous sections of PLA which also led to improved dispersion of CNCs. Figure 7(b), shows
504 slight change in the slope near T_g with complete absence of the cold crystallization peak for
505 PLA-*g*-CNC in comparison to the neat PLA. Occurrence of such phenomenon is probably due to
506 formation of enhanced cross-linked structures of the amorphous PLA with the CNC domains
507 which restricts the amorphous polymer chain mobility to form crystalline lamella. The high
508 density of cross-linked PLA chains with crystalline CNC through C-C bond formation, leads to
509 better interfacial adhesion, subsequently reduces the interspaces causing reduction in the free
510 volume. During the 2^{nd} heating cycle, relatively more amorphous PLA chains became
511 crystallized at T_{cc}~125°C; however, cold crystallization peaks were absent in case of grafted
512 PLAs for all CNC loadings due to already developed crystallites during the first cooling as
513 shown in Figure 7(a). These thermographs clearly depict that the activation energy of chain
514 folding is lower in PLA-*g*-CNC compared to pristine PLA due to which grafted PLA chains
515 could overcome the energy barrier and crystallize upon cooling whereas neat PLA chains could
516 not [25]. The melting peaks for PLA-*g*-CNCs showed a narrow and sharper peak compared to
517 PLA which suggests formation of stable and uniform size crystals during reactive extrusion
518 process. These findings are in line with GPC studies where relatively uniform MWD of the PLA-

519 *g*-CNC chains was observed due to which these samples show the single melting phenomenon
520 compared to pristine PLA.
521 Further, DSC analysis was done for extracted PLA-*g*-CNC gel domains which are reprocessed
522 under similar extrusion conditions (Figure 8 (a) & (b)). The re-extruded PLA-*g*-CNC showed
523 drastic reduction in the % *g*-PLA and X_c values (Table 2), which is due to chain scissions under
524 high shear thermal stressed conditions. The % of PLA chains grafted onto the CNC surface after
525 reprocessing of the PLA-g-CNC gels (*g*-rPLA) was calculated from the ratio of C_p value of the
526 reprocessed rPLACNC nanocomposite to the C_p value of reprocessed PLA corresponding to their
527 T_g values. The reduction in *g*-rPLA values suggests possible debonding/ degradation of the high
528 molecular weight amorphous PLA chains grafted on the CNC surface, which subsequently leads
529 to decrease in X_c. The crystallization peak temperature increases with increase in CNC loading
530 for the reprocessed samples. It is probably because on re-extrusion of PLA/CNC nanocomposites
531 the fraction of gel domains containing agglomerated CNCs increased and it underwent molecular
532 weight reduction due to thermal degradation. Presence of such agglomerations and gel fractions
533 hindered the crystallization phenomena which led to shift in T_c ~ 126.3ºC for rPLA to 130.2ºC
534 for rPLACNC2(3.33). However, the reprocessed PLA/CNC nanocomposites do not show any
535 significant alteration in melting behavior compared to PLA-*g*-CNC. Therefore, it can be
536 concluded that while reactive grafting of CNCs leads to significant change in the crystallization
537 properties, both the integrity and stability of the crystal structures are maintained after
538 reprocessing.
539 *Mechanical property investigations*
540 The mechanical properties of *in situ* reactive compatibilized PLA-*g*-CNC were investigated to
541 study the effect of grafting nanofillers like CNC in the presence of DCP. The neat PLA extruded

strips have an ultimate tensile strength (UTS) of 36.2 MPa and elongation at break of 9%, comparable with the reported literature [46]. The PLA extruded strips with 1wt. % of CNC (PLACNC1) in the absence of the DCP as cross-liking agent, showed improvement in the UTS Young's modulus (YM) by ~14 and ~100% respectively. Reactive grafting of CNCs into PLA matrix led to significant increase in the tensile strength and YM of nanocomposite by ~41% and ~490% respectively (Figure 9 (a) & (c)). However, the elongation at break is reduced significantly (by ~ 70%) for all the loading fractions of CNCs studied. Restriction in the elongation may be due to the crosslinking between CNCs and the polymer chains through the formation of C–C bond linkages (Figure 9 (b)). However, the improvement in modulus can be explained by the following two phenomena: firstly, reactive grafting of PLA chains on CNC surface leads to uniform dispersion and enhances interfacial adhesion of PLA-modified-CNCs with the bulk PLA matrix (as explained in previous section), and secondly, the formation of C–C bonds between the PLA and CNC could act as an effective linkage for transferring the developed stresses (transverse elastic modulus of 18–50 GPa and anisotropic elastic modulus of 140–220 GPa [9] of individual CNCs) between them. Also, increase in the MWD during reactive extrusion and formation of branched network like structures in PLA-*g*-CNC probably contributes to the increase in the modulus. Moreover, as explained from the FTIR studies, grafting of crystalline segments of CNCs probably took place on the amorphous domains of PLA, which subsequently led to increase in the crystalline fractions in the PLA-*g*-CNC nanocomposites (further confirmed by XRD studies). Presence of such crosslinking with the amorphous segments restricts the free mobility of PLA chains to dissipate energy under tensile force, resulting in the increased brittleness and reduction in the % elongation at break. However, on increasing the % CNC loading (up to ~3wt%) in PLA-*g*-CNC nanocomposites, grafting

565 efficiency decreases due to agglomeration of CNC which subsequently leads to deterioration of
566 mechanical properties. It is noteworthy to mention that similar phenomenon of decrease in
567 elongation for such cross-linked structures was also observed in the case of the reactive extruded
568 polyhydroxybutyrate and polypropylene samples [47].

569 When the extracted PLA-*g*-CNC gels were reprocessed into strips under identical processing
570 conditions (at 180ºC, 50 rpm and retention time of 5 mins), the UTS and modulus of the rPLA-*g*-
571 CNC films decreased by ~28 and 56% respectively (Figure9 (a) & (c)). This is probably because
572 degradation of bulk PLA chains (both branched and linear) takes place either during thermal
573 reprocessing or due to the presence of sulfate groups on the agglomerated CNCs (at higher
574 loadings), as confirmed by the MWD studies. It is noteworthy to mention that the UTS for the
575 reprocessed samples at different wt. % CNC loadings are comparable to neat PLA or PLACNC1,
576 probably due to shielding of sulphate groups. Presence of grafted PLA chains on the CNC
577 surface helped overcome the problems related to thermal induced PLA degradation during
578 extrusion in presence of CNCs especially at higher loadings. MWD analysis of the reprocessed
579 PLA-*g*-CNC films shows decrease in M_w and M_n by ~18 and 15% respectively and decrease in
580 the area of the high molecular weight peaks from ~89 to 68% (Figure S2), which could be
581 responsible for the decrease in mechanical properties. However, the increase in overall content of
582 the CNCs are represented in brackets for the reprocessed PLA-*g*-CNC samples (due to removal
583 of ungrafted PLA chains while washing). It could help in improving the UTS of the
584 nanocomposites but its contribution towards the nanocomposites have been found to be
585 negligible. The reprocessed films showed slight improvement in elongation at break (by ~75%),
586 probably because of the presence of low molecular weight fractions (increase in the area of low
587 molecular weight fractions after reprocessing) which act as plasticizers under tensile load. The

588 UTS and modulus values of the reprocessed/recycled PLA-*g*-CNC films are comparable or even
589 better than PLA (especially Young's modulus). Therefore, the approach of grafting PLA chains
590 onto CNCs through reactive extrusion process allows the recycling of PLA-*g*-CNC
591 nanocomposite films even after service life.

592 Fracture behavior of the stretched PLA-*g*-CNCs films prepared using original and reprocessed
593 PLA/CNC samples was studied. FESEM micrographs of PLADCNC1 films showed presence of
594 large polymer fibrillation which is caused by the formation of enhanced cross-linking (Figure
595 10(a)). Small micro-gel beads of PLA-*g*-CNC were also found along with fibrils, consistent with
596 reported studies for reactively grafted polymers [25]. Branching of PLA chains in the presence of
597 DCP leads to formation of entangled fibrils which hinders early matrix failure, thereby
598 increasing its toughness effectively. Therefore, it could be concluded that both enhancement in
599 interfacial adhesion and formation of such entangled branched structures are responsible for the
600 improvement in mechanical properties of PLA-*g*-CNC. However, on reprocessing of the
601 extracted gels, rPLACNC1(1.35) films showed smooth prominent rigid lines parallel to the
602 direction of the tensile load (Figure 10(b)). Presence of such aligned fibrils in reprocessed films
603 is due to the mobility of branched polymer chains which causes certain improvement in the
604 elongation properties. Therefore, it can be concluded that reactive extrusion of PLA/CNC
605 nanocomposites by varying the DCP and CNC concentrations will lead to different degree of
606 chain grafting and branching which can be used to tune the mechanical properties.

607 *Thermo-mechanical studies*

608 Dynamic mechanical analysis (DMA) was carried out to measure the change in the storage
609 modulus (E') and tan (δ) before and after reprocessing of the PLA-*g*-CNC nanocomposites (at ~2
610 wt% CNC loading) over a temperature range of 25–90ºC (Figure 11 (a) & (b)). The E' increased

on incorporation of CNC (at 2 wt. %) in presence of DCP due to the formation of cross-linked structure and better interfacial adhesion with the polymer matrix. E' values for reactively grafted CNCs is found to be significantly higher than the ungrafted PLA/CNC films. This suggests that grafting of CNCs with polymer through the formation of the C–C bond leads to effective transfer of CNC modulus to the PLA matrix. The effectiveness of the grafted CNCs as reinforcement agent is further measured by the filler effectiveness coefficient C_{FE}:

$$C_{FE} = \left(\frac{E'_g}{E'_r}\right)_{comp} / \left(\frac{E'_g}{E'_r}\right)_{matrix}$$

where E'_g and E'_r represent the storage moduli for the glassy and rubbery state of PLA and the PLA-*g*-CNC nanocomposite, measured at constant frequency of 1Hz and at temperature 46ºC and 85ºC respectively [22]. The nanofillers which have lower C_{FE} values are considered to be the most effective reinforcing agent for the given polymer matrix. The C_{FE} values for the PLA/CNC films with ~2 wt % CNC (PLACNC2) fabricated through traditional approach was 0.836, compared to 0.721 for the reactively grafted PLA-*g*-CNC (at ~2 wt %). Therefore, it can be concluded from the C_{FE} data that effective dispersion of CNCs could be achieved using the proposed reactive grafting approach.

Figure 11(b) shows the comparison of the tan (δ) plots for which the peak temperature was selected to be the glass transition temperature for the nanocomposite. It is found that the glass transition temperature decreases for the reactively extruded PLA-*g*-CNC nanocomposites in comparison to the neat PLA. This is probably because the cross-linked PLA-*g*-CNC gels usually undergoes heat shrinkage at T_g (as explained in previous section), which depends on the degree of branching as per the reported literature [44]. The decrease in T_g was further confirmed by DSC analysis and similar phenomenon has been previously observed for the reactive grafting of maleic anhydride on PLA in the presence of DCP [26].

On reprocessing E' decreases significantly, probably due to the thermal degradation which is accompanied by a decrease in the molecular weight and formation of large fractions of low molecular weight chains which are less effective at storing energy under tensile load. However, C_{FE} values do not change significantly during reprocessing of the PLA-*g*-CNC films suggesting that there is no significant change in the grafted CNC structure, as discussed earlier. Therefore, it can be concluded from the thermo-mechanical studies that reactive grafting of CNCs results in the formation of thermally stable and reprocessible PLA films suited for high performance engineering applications.

Conclusions

This work successfully demonstrated the grafting of PLA on CNC using DCP initiator via reactive extrusion process which enhances the compatibilization between hydrophobic PLA and hydrophilic CNC. The maximum fraction of PLA chains grafted on CNC surface is 66% with the highest grafting efficiency achieved at 1 wt% CNC loadings. NMR and FTIR spectroscopic studies confirm the grafting between the methine (-CH) groups of PLA with the methylene groups of CNC by establishing C–C bridge using DCP as grafting agent. Due to the chain extensions and formation of branched structures, the M_w and M_n of PLA-*g*-CNCs increased significantly. Interestingly, M_w and M_n do not change significantly during recycling of the PLA-*g*-CNC gels. Both PLA-*g*-CNC (obtained through reactive extrusion) and rPLACNC (obtained after further reprocessing) are capable of forming transparent films with improved adhesion and dispersion of CNCs. Due to formation of the C–C bonds with the CNCs, both the thermal stability and the mechanical properties of PLA-*g*-CNC nanocomposites improved significantly. The tensile strength and Young's modulus improved by 41and 490% respectively, whereas the filler effectiveness coefficient (C_{FE}) values decreased, suggesting that the grafted CNCs act as an

656 efficient reinforcing agent. XRD and DSC studies shows improvement in crystallinity, possibly
657 due to grafting of the amorphous PLA chains onto the crystalline CNC segments which act as
658 nucleating agent. This novel, thermally stable, reactive extrusion-based strategy can be
659 implemented for industrial scale fabrication of PLA-*g*-CNC recyclable biocomposite films for
660 potential applications in packaging.

661 **Acknowledgements**

662 Authors acknowledge the research grant from Department of Biotechnology, Ministry of
663 Science and Technology, India (BT/345/NE/TBP/2012). Authors would also like to express
664 sincere thanks to the Centre of Excellence for Sustainable Polymers (CoESuSPol) funded by the
665 Department of Chemicals and Petrochemicals, Government of India, and the Central Instruments
666 Facility, Indian Institute of Technology, Guwahati, India for the analytical facilities.

667

668 **References**

669 [1] B. Gupta, N. Revagade, J. Hilborn, Prog. Polym. Sci. 32 (2007) 455–482.
670 [2] M.M. Reddy, S. Vivekanandhan, M. Misra, S.K. Bhatia, A.K. Mohanty, Prog. Polym. Sci.
671 38 (2013) 1653–1689.
672 [3] K. Madhavan Nampoothiri, N.R. Nair, R.P. John, Bioresour. Technol. 101 (2010) 8493–
673 8501.
674 [4] H. Li, M.A. Huneault, Polymer 48 (2007) 6855–6866.
675 [5] A.P.M. Natalia Herrera, Compos. Sci. Technol. 106 (2014).
676 [6] L. Yu, K. Dean, L. Li, Prog. Polym. Sci. 31 (2006) 576–602.
677 [7] T. Maharana, B. Mohanty, Y.S. Negi, Prog. Polym. Sci. 34 (2009) 99–124.
678 [8] A. Södergård, M. Stolt, Prog. Polym. Sci. 27 (2002) 1123–1163.

[9] R.R. Lahiji, X. Xu, R. Reifenberger, A. Raman, A. Rudie, R.J. Moon, Langmuir 26 (2010) 4480–4488.

[10] P. Dhar, D. Tarafder, A. Kumar, V. Katiyar, RSC Adv. 5 (2015) 60426–60440.

[11] S. Montanari, M. Roumani, L. Heux, M.R. Vignon, Macromolecules 38 (2005) 1665–1671.

[12] M. Salajková, L.A. Berglund, Q. Zhou, J. Mater. Chem. 22 (2012) 19798–19805.

[13] S. Spinella, G. Lo Re, B. Liu, J. Dorgan, Y. Habibi, P. Leclère, J.-M. Raquez, P. Dubois, R.A. Gross, Polymer 65 (2015) 9–17.

[14] T. Mukherjee, M. Sani, N. Kao, R.K. Gupta, N. Quazi, S. Bhattacharya, Chem. Eng. Sci. 101 (2013) 655–662.

[15] M. de O. Taipina, M.M.F. Ferrarezi, I.V.P. Yoshida, M. do C. Gonçalves, Cellulose 20 (2013) 217–226.

[16] M. Hirota, N. Tamura, T. Saito, A. Isogai, Cellulose 19 (2012) 435–442.

[17] A. Saralegi, M.L. Gonzalez, A. Valea, A. Eceiza, M.A. Corcuera, Compos. Sci. Technol. 92 (2014) 27–33.

[18] D. Bondeson, K. Oksman, Compos. Interfaces 14 (2007) 617–630.

[19] K. Ben Azouz, E.C. Ramires, W. Van den Fonteyne, N. El Kissi, A. Dufresne, ACS Macro Lett. 1 (2012) 236–240.

[20] V. Khoshkava, M.R. Kamal, Powder Technol. 261 (2014) 288–298.

[21] N. Lin, A. Dufresne, Macromolecules 46 (2013) 5570–5583.

[22] M. Pracella, M.M.-U. Haque, D. Puglia, Polymer 55 (2014) 3720–3728.

[23] W. Yang, F. Dominici, E. Fortunati, J.M. Kenny, D. Puglia, RSC Adv. 5 (2015) 32350–32357.

[24] P. Ma, X. Cai, Y. Zhang, S. Wang, W. Dong, M. Chen, P.J. Lemstra, Polym. Degrad. Stab. 102 (2014) 145–151.

[25] Y. Bian, C. Han, L. Han, H. Lin, H. Zhang, J. Bian, L. Dong, RSC Adv. 4 (2014) 41722–41733.

[26] S.W. Hwang, S.B. Lee, C.K. Lee, J.Y. Lee, J.K. Shim, S.E.M. Selke, H. Soto-Valdez, L. Matuana, M. Rubino, R. Auras, Polym. Test. 31 (2012) 333–344.

[27] Y.-M. Corre, J. Duchet, J. Reignier, A. Maazouz, Rheol. Acta 50 (2011) 613–629.

[28] E.P. Katherine M. Dean, J. Polym. Environ. 20 (2012).

[29] M.B. Khajeheian, A. Rosling, J. Polym. Environ. 23 (2014) 62–71.

[30] L. Wei, A.G. McDonald, N.M. Stark, Biomacromolecules 16 (2015) 1040–1049.

[31] P. Dhar, U. Bhardwaj, A. Kumar, V. Katiyar, Polym. Eng. Sci. (2015).

[32] P. Dhar, A. Kumar, V. Katiyar, Cellulose (2015) 1–17.

[33] E.M. Dannenberg, M.E. Jordan, H.M. Cole, J. Polym. Sci. 31 (1958) 127–153.

[34] M. Takamura, T. Nakamura, T. Takahashi, K. Koyama, Polym. Degrad. Stab. 93 (2008) 1909–1916.

[35] M.-B. Coltelli, S. Bronco, C. Chinea, Polym. Degrad. Stab. 95 (2010) 332–341.

[36] Y. Liu, X. Jin, X. Zhang, M. Han, S. Ji, Carbohydr. Polym. 117 (2015) 312–318.

[37] L.T. Sin, A.R. Rahmat, W.A.W.A. Rahman, Polylactic Acid: PLA Biopolymer Technology and Applications, William Andrew, 2012.

[38] Á. Csikós, G. Faludi, A. Domján, K. Renner, J. Móczó, B. Pukánszky, Eur. Polym. J. 68 (2015) 592–600.

[39] K. Choi, M.-C. Choi, D.-H. Han, T.-S. Park, C.-S. Ha, Eur. Polym. J. 49 (2013) 2356–2364.

723 [40] K.-M. Choi, S.-W. Lim, M.-C. Choi, D.-H. Han, C.-S. Ha, Macromol. Res. 22 (2014)
724 1312–1319.
725 [41] T. Furukawa, H. Sato, R. Murakami, J. Zhang, Y.-X. Duan, I. Noda, S. Ochiai, Y. Ozaki,
726 Macromolecules 38 (2005) 6445–6454.
727 [42] J. Liu, S. Zhang, L. Zhang, Y. Bai, Polymer 55 (2014) 2472–2480.
728 [43] N. Lin, J. Huang, P.R. Chang, J. Feng, J. Yu, Carbohydr. Polym. 83 (2011) 1834–1842.
729 [44] Y. Bian, L. Han, C. Han, H. Lin, H. Zhang, J. Bian, L. Dong, CrystEngComm 16 (2014)
730 2702–2714.
731 [45] J.O. Zoppe, Y. Habibi, O.J. Rojas, R.A. Venditti, L.-S. Johansson, K. Efimenko, M.
732 Österberg, J. Laine, Biomacromolecules 11 (2010) 2683–2691.
733 [46] N. Najafi, M.C. Heuzey, P.J. Carreau, Compos. Sci. Technol. 72 (2012) 608–615.
734 [47] L. Wei, N.M. Stark, A.G. McDonald, Green Chem. (2015).
735

736 Figures and Tables

737 Scheme 1: (a) Mechanism of thermal decomposition of the DCP into peroxide radicals during
738 extrusion at T=180ºC (initiation step), (b) Generation of CNC and PLA radicals followed by
739 reactive extrusion at screw speed = 50 rpm and recycle time= 2 min (propagation step) leading to
740 the formation of PLA grafted CNC structures (termination step). (c) Pictorial representation of
741 the grafting mechanism of initiation, propagation and termination of the reactive extrusion
742 process for PLA-*g*-CNC along the different zones of the extruder.

743 Figure 1: (a) Comparison of FTIR spectrograms of neat PLA, PLAD, PLADCNC1and rPLA
744 CNC1(1.35) with the selected regions (marked in black boxes) analyzed at (b) 3600–2700 cm^{-1},

(c) 1900–1400 cm^{-1} and (d) 1500–600 cm^{-1} wavenumber range and the representative peaks marked with black arrows.

Figure 3: (a) Molecular weight distribution, weight average (M_w) and number average (M_n) and (b) polydispersity index (PDI) of extruded PLA, reactively extruded PLA/CNC nanocomposites (PLAD, PLADCNC1, PLADCNC2 & PLADCNC3) and reprocessed PLA-*g*-CNC gels (rPLA, rPLACNC1(1.35), rPLACNC2(3.33) & rPLACNC3(5.15)).

Figure 4: (a) Pictorial comparisons of the neat PLA, PLADCNC1 and rPLACNC1strips with PLA/CNC 1wt. % extruded by simple melt blending (traditional approach), (b) FESEM micrographs of PLADCNC1 and (c) rPLACNC1(1.35).

Figure 5: Comparison of the thermogravimetric (TGA) plots for the neat PLA, PLADCNC1 and rPLACNC1(1.35) respectively with the inset showing the TGA profile in the temperature range of 345–375ºC.

Figure 6: XRD diffractograms for the extruded neat PLA and reactively extruded PLA-*g*-CNC films, represented as PLAD, PLADCNC1and PLADCNC2.

Figure 7: DSC thermograms for the (a) first cooling cycle and (b) second heating cycle for the reactively grafted PLA-*g*-CNC nanocomposites.

Figure 8: DSC thermograms for the (a) first cooling cycle and (b) second heating cycle for the re-extruded PLA-*g*-CNC gels.

Figure 9: Mechanical properties: (a) ultimate tensile strength, (b) % elongation and (c) Young's modulus of the reactively extruded PLA-*g*-CNC nanocomposites and reprocessed PLA-*g*-CNC gels.

766 Figure 10: FESEM micrographs of the fractured samples of (a) PLADCNC1 and (b)
767 rPLACNC1(1.35).

768 Figure 11: (a) DMA and (b) tan δ plots for the reactively grafted and reprocessed PLA-*g*-CNC
769 films (~2 wt% CNC loading).

770

Figure 2: ^{1}H NMR spectra for the PLA-*g*-CNC sample (PLADCNC1) with the selected region (4.4–3.3 ppm, marked in black box; as zoomed) and shown as inset. The inset also shows the probable structure of PLA-*g*-CNC formed after reactive extrusion in the presence of DCP.

Table 1: Calculated grafting parameters, namely gel yield percentage (Gel Yield), graft percentage (%GP), grafting efficiency (%GE) and weight conversion (%WC), for the reactively extruded PLA/CNC nanocomposite strips in the presence of DCP (1.2 wt%). The effect of grafting on the change in the specific rotation and optical rotation are also listed.

Samples	Gel Yield (%)	Graft (%)	Graft Efficiency (%)	Weight Conversion (%)	Specific Rotation (°)	Optical Rotation (°)
PLA	-	-	-	-	-158.37	-1.582
PLAD	52.2(±0.6)	-	-	50.8(±1.8)	-145.07	-1.509
PLADCNC1	74.2(±0..9)	7706.2(±10.3)	76.8(±2.9)	73.6(±2.1)	-137.24	-1.329
PLADCNC2	61.0(±1.2)	2900.1(±25.5)	57.6(±5.1)	59.6(±1.9)	-140.73	-1.419
PLADCNC3	58.1(±1.8)	1840.0(±21.3)	54.7(±2.8)	57.7(±1.7)	-145.22	-1.475

Table 2: Thermal and crystallization properties of the reactively extruded PLA-*g*-CNC nanocomposites and reprocessed PLA-*g*-CNC gels.

Sample	T_g (°C)	$\Delta C_{p,Tg}$ (J/g.°C)	T_{cc} (°C)	ΔH_{cc} (J/g)	T_c (°C)	ΔH_c (J/g)	T_m (°C)	ΔH^a_m (J/g)	X_c (%)	*g*-PLA (*g*-rPLA) (%)
PLA	61.6	1.638	112.5	26.2	-	-	170.2	-26.1	28.1	100
PLAD	54.5	0.780	91.6	13.8	127.0	27.4	168.6	-29.2	31.3	47.6
PLADCNC1	52.7	1.080	88.0	12.1	127.3	24.0	165.5	-31.6	34.0	66.0
PLADCNC2	55.0	0.823	93.3	16.6	125.3	28.8	169.1	-32.5	35.0	50.2
PLADCNC3	55.8	0.875	93.5	15.5	124.3	28.9	169.8	-31.2	33.5	53.4
rPLA	53.0	0.944	91.5	14.7	126.3	29.3	169.0	-29.2	31.3	-
rPLACNC1(1.35)	57.0	0.885	94.2	14.1	125.0	26.0	169.7	-26.7	28.7	54.0(93.7)
rPLACNC2(3.33)	56.0	0.850	90.6	11.7	130.2	24.7	167.7	-30.6	32.9	51.9(90.0)
rPLACNC3(5.15)	55.8	0.781	90.6	12.9	129.9	29.2	166.4	-31.0	33.3	47.6(82.7)

where T_g= glass transition temperature, $\Delta C_{p,Tg}$=specific heat corresponding to glass transition temperature calculated from first heating cycle, *g*-PLA=represents the % of PLA chains grafted onto CNC surface (measured as the ratio of $\Delta C_{p,Tg}$ (for PLA-*g*-CNC gels)/ $\Delta C_{p,Tg}$ (for PLA)), *g*-rPLA= represents the % of PLA chains grafted onto CNC surface after reprocessing of the PLA-*g*-CNC gels (measured as the ratio of $\Delta C_{p,Tg}$ (for reprocessed rPLACNC nanocomposites)/ $\Delta C_{p,Tg}$ (for rPLA)), T_{cc}= cold crystallization temperature, ΔH_{cc}= enthalpy for cold crystallization, T_c= crystallization temperature (cooling cycle), T_m= melting temperature, ΔH^a_m= melting enthalpy corresponding to 2nd heating cycle, ΔH^o_m = melting enthalpy for 100% crystalline PLA was taken as 93 J/g [26] and X_c=degree of final crystallinity calculated from ratio of ΔH^a_m and ΔH^o_m .

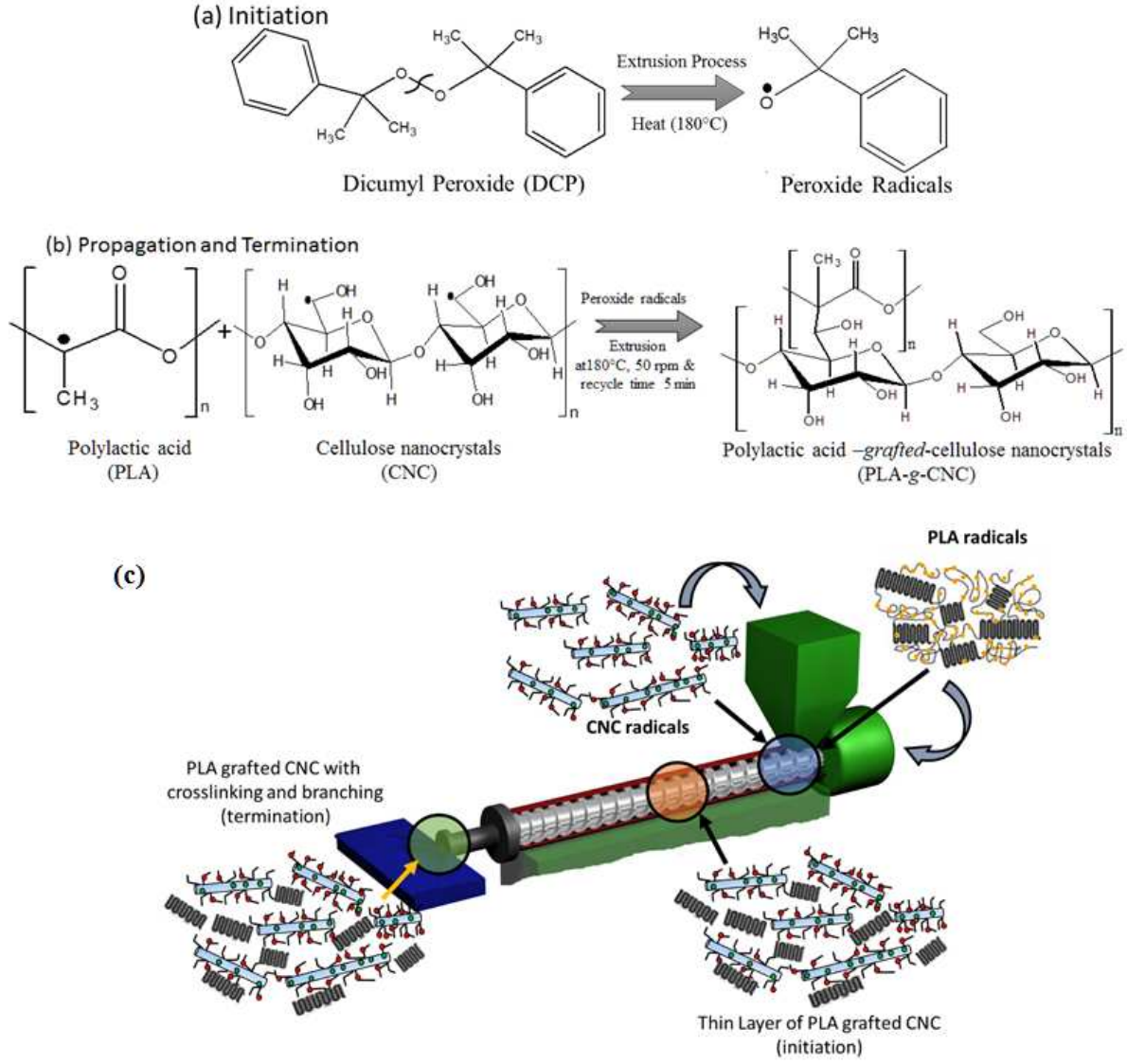

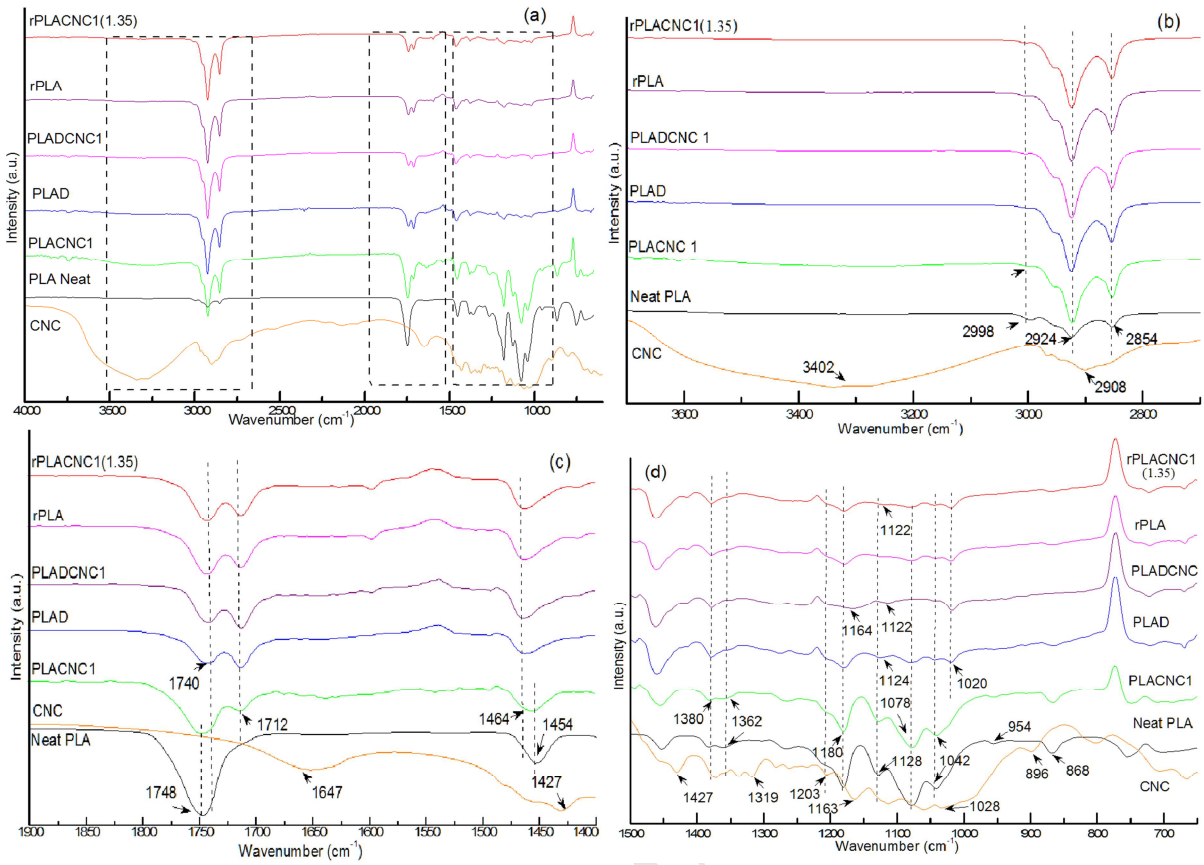

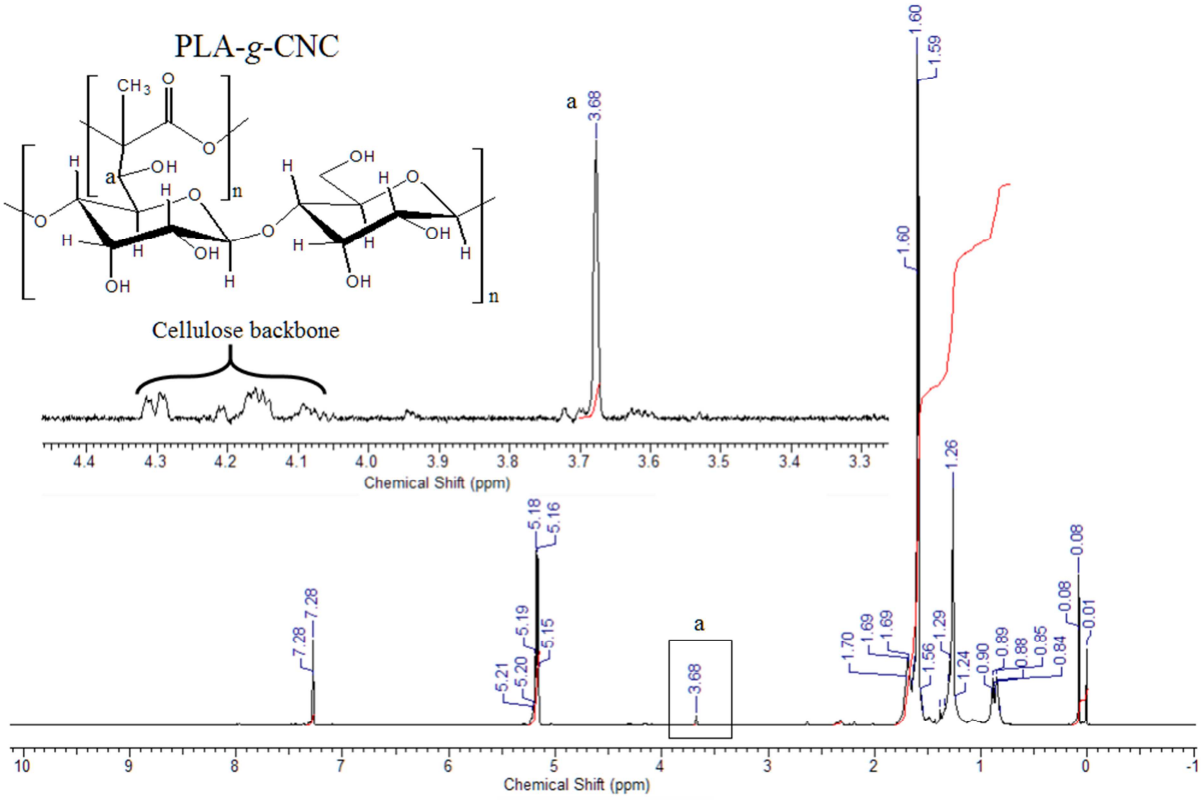

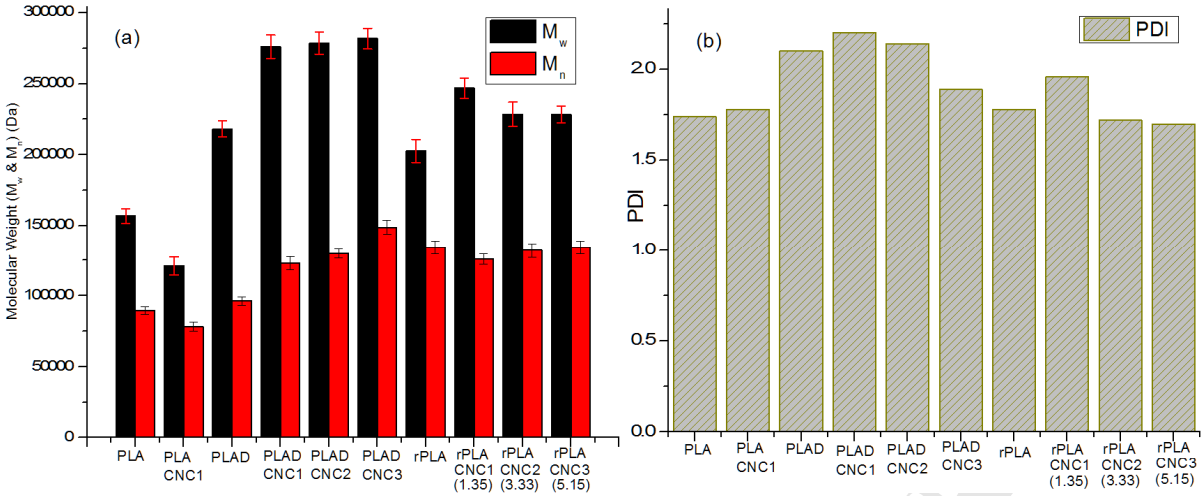

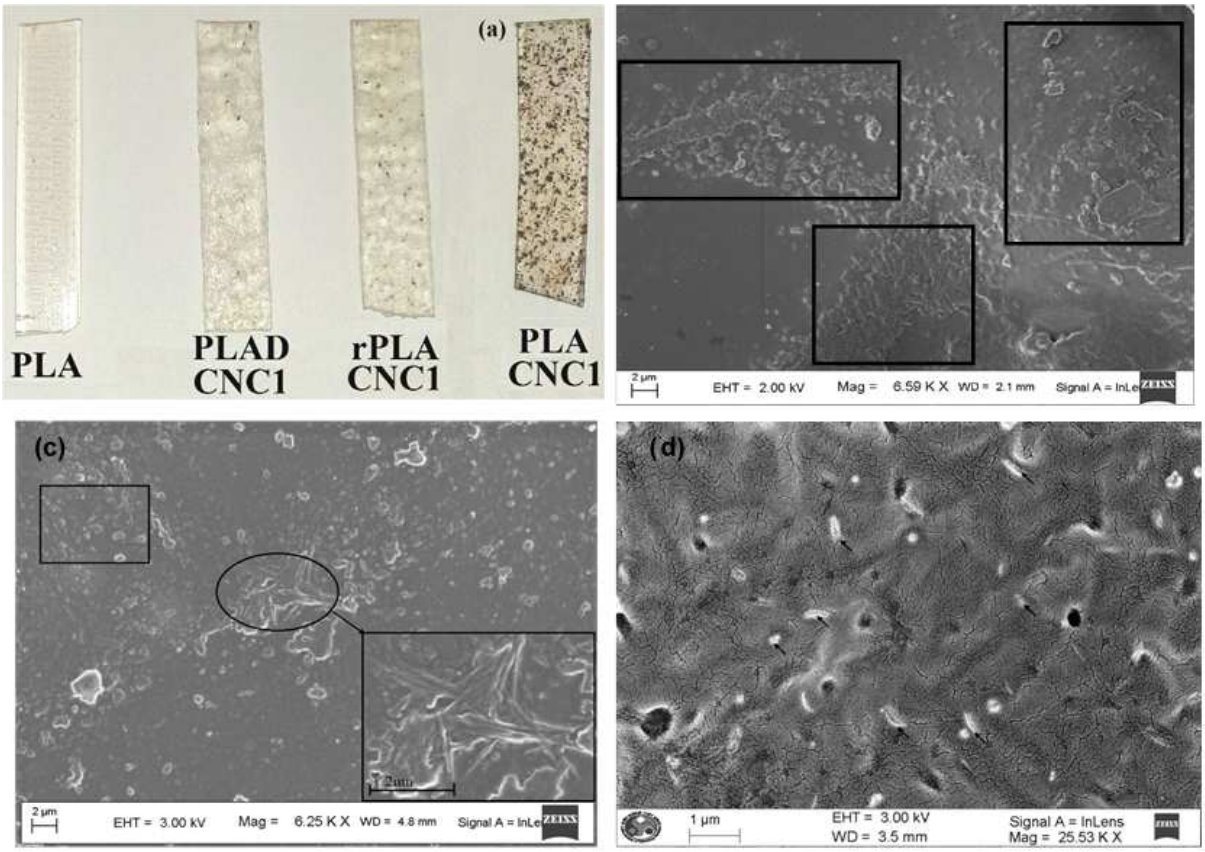

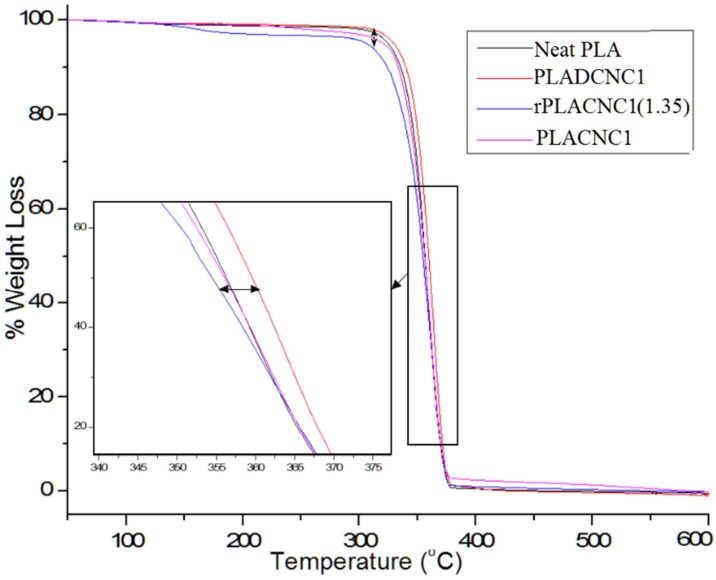

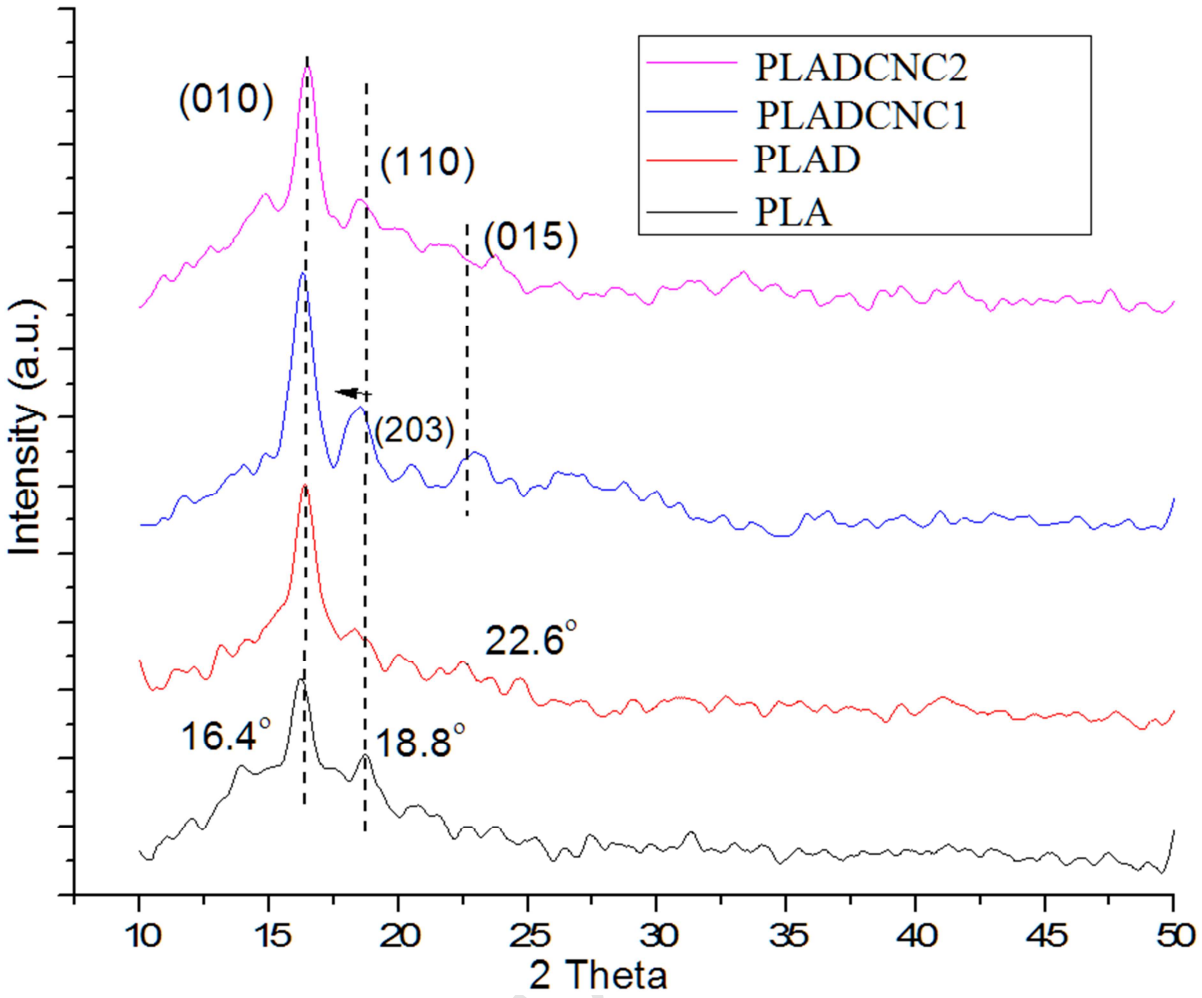
PLADCNC2
PLADCNC1
PLAD
PLA
(010)
(110)
(015)
(203)
22.6°
16.4°
18.8°
Intensity (a.u.)
2 Theta
10
15
20
25
30
35
40
45
50

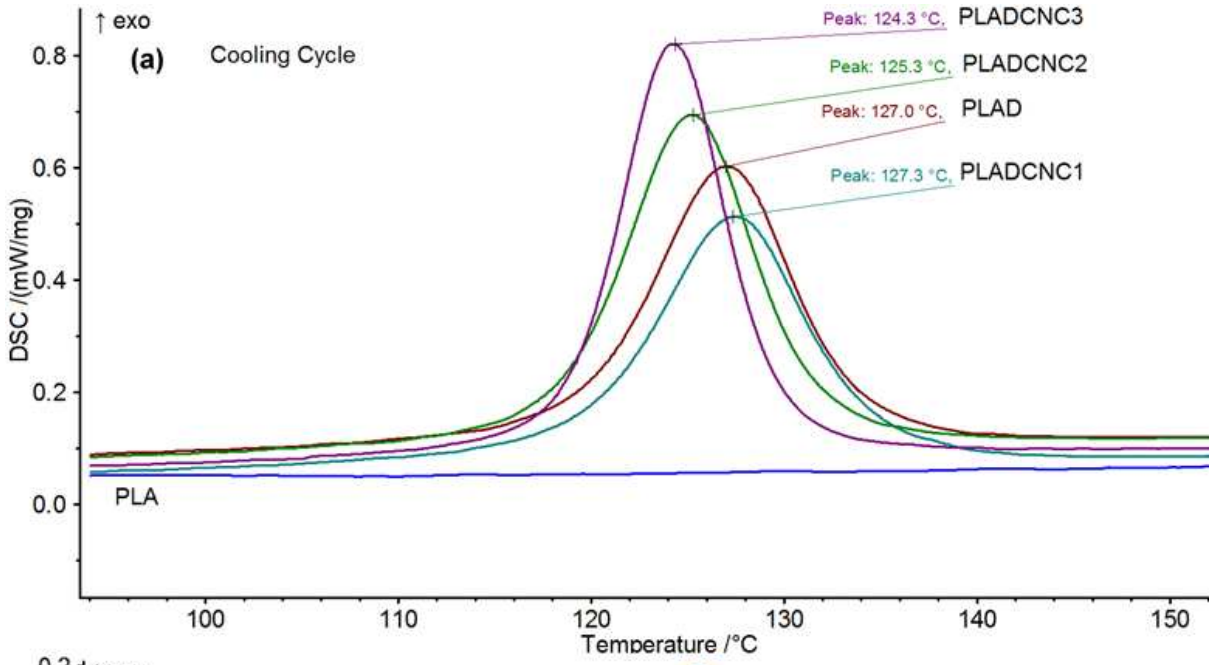
↑ exo
(a) Cooling Cycle
Peak: 124.3 °C, PLADCNC3
Peak: 125.3 °C, PLADCNC2
Peak: 127.0 °C, PLAD
Peak: 127.3 °C, PLADCNC1
PLA
DSC /(mW/mg)
Temperature /°C

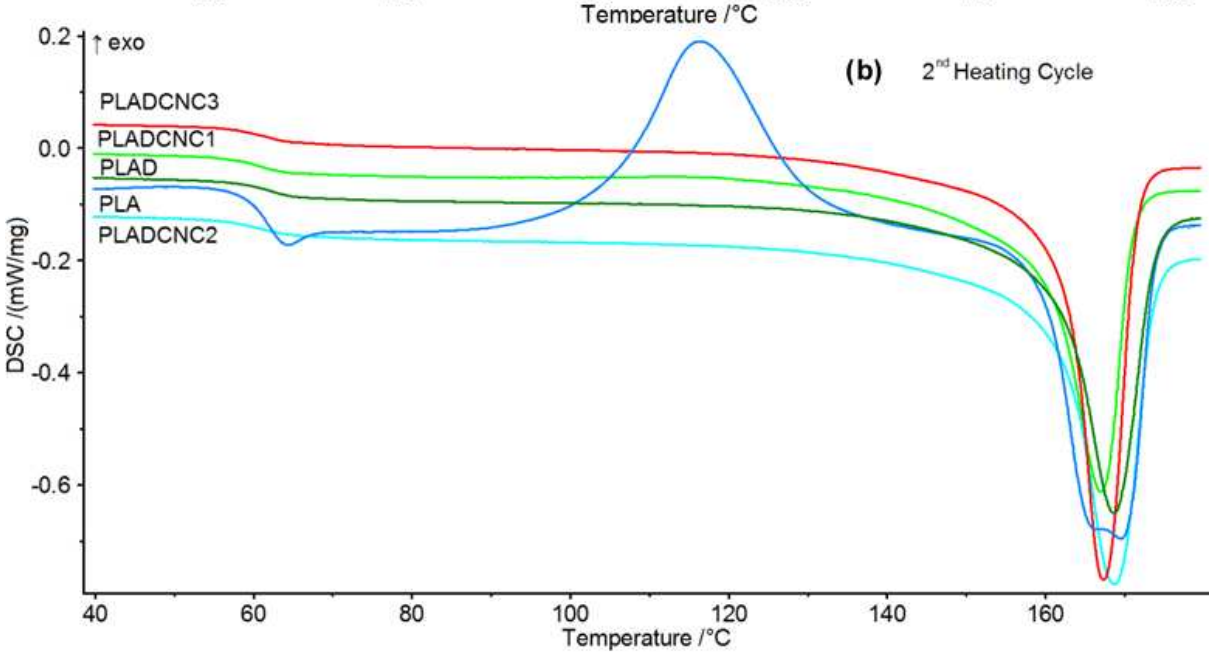
↑ exo
(b) 2nd Heating Cycle
PLADCNC3
PLADCNC1
PLAD
PLA
PLADCNC2
DSC /(mW/mg)
Temperature /°C

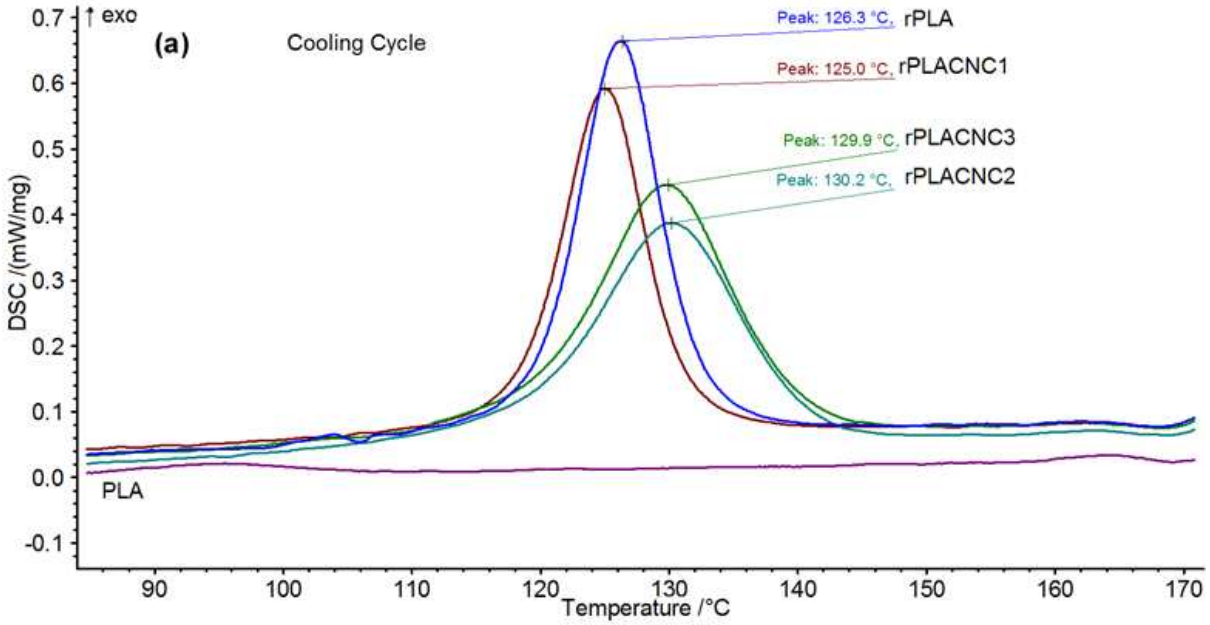
↑ exo
(a)
Cooling Cycle
Peak: 126.3 °C, rPLA
Peak: 125.0 °C, rPLACNC1
Peak: 129.9 °C, rPLACNC3
Peak: 130.2 °C, rPLACNC2
PLA
DSC /(mW/mg)
Temperature /°C

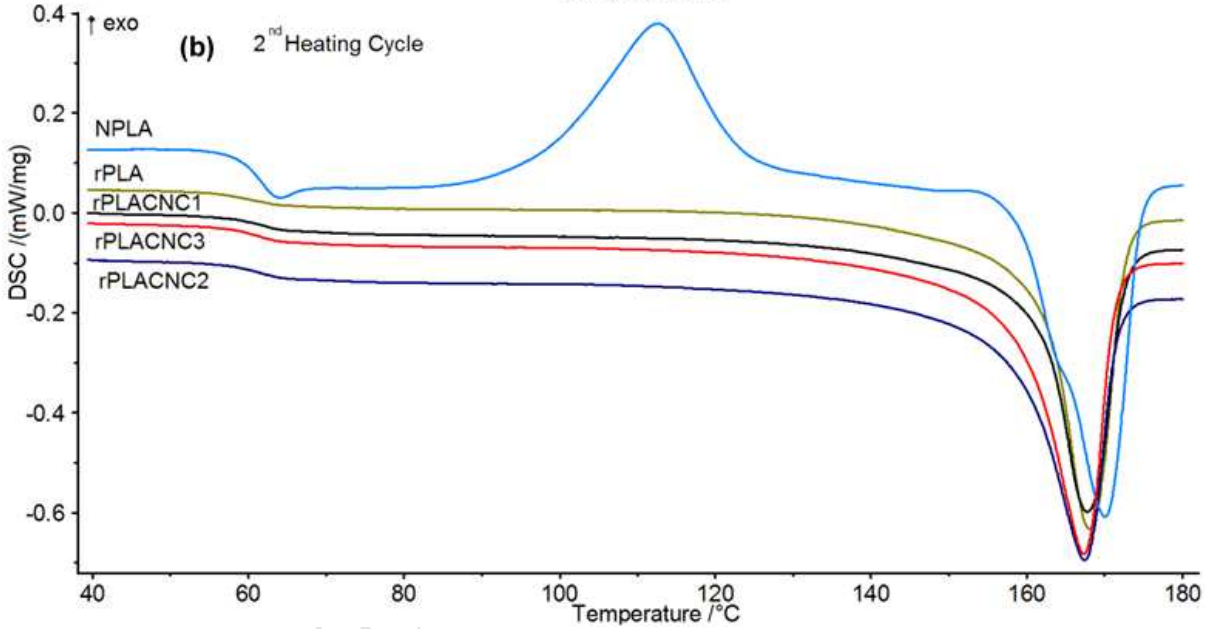
↑ exo
(b)
2nd Heating Cycle
NPLA
rPLA
rPLACNC1
rPLACNC3
rPLACNC2
DSC /(mW/mg)
Temperature /°C

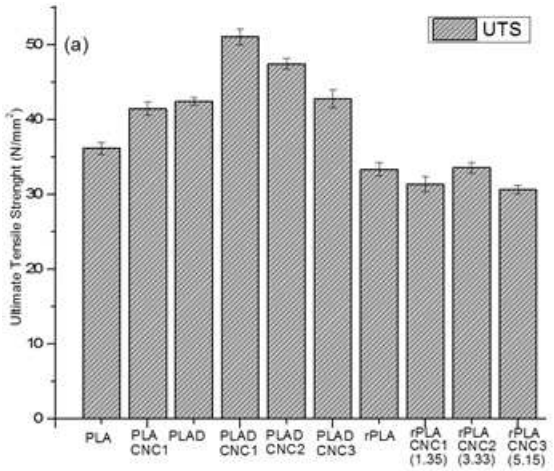
(a)
UTS
Ultimate Tensile Strenght (N/mm²)
0
10
20
30
40
50
PLA
PLA CNC1
PLAD
PLAD CNC1
PLAD CNC2
PLAD CNC3
rPLA
rPLA CNC1 (1.35)
rPLA CNC2 (3.33)
rPLA CNC3 (5.15)

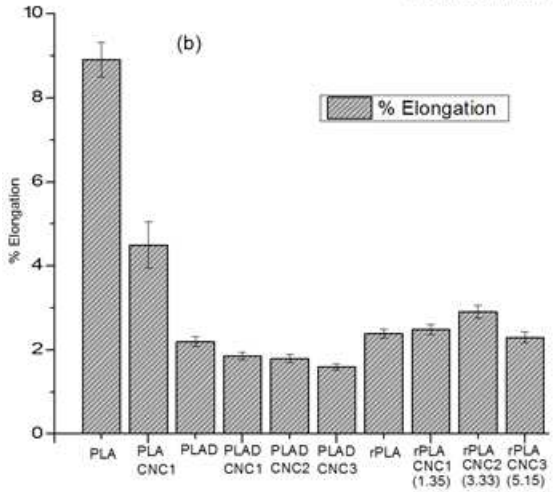
(b)
% Elongation
% Elongation
0
2
4
6
8
10
PLA
PLA CNC1
PLAD
PLAD CNC1
PLAD CNC2
PLAD CNC3
rPLA
rPLA CNC1 (1.35)
rPLA CNC2 (3.33)
rPLA CNC3 (5.15)

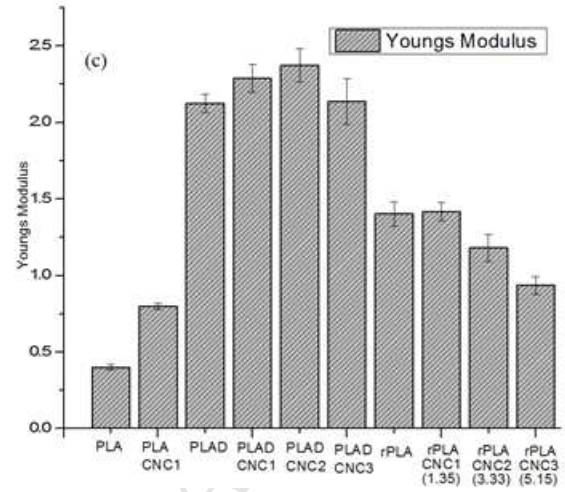
(c)
Youngs Modulus
Youngs Modulus
0.0
0.5
1.0
1.5
2.0
2.5
PLA
PLA CNC1
PLAD
PLAD CNC1
PLAD CNC2
PLAD CNC3
rPLA
rPLA CNC1 (1.35)
rPLA CNC2 (3.33)
rPLA CNC3 (5.15)

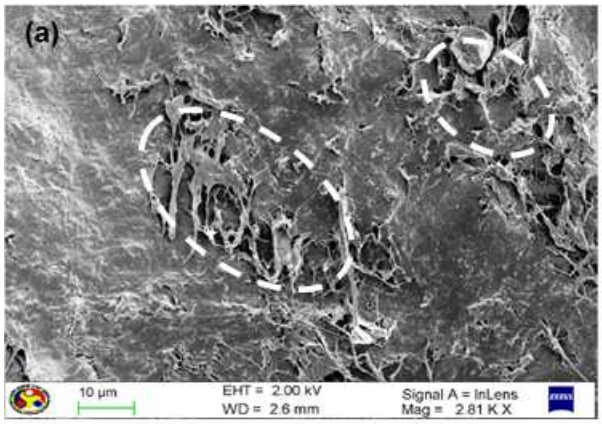

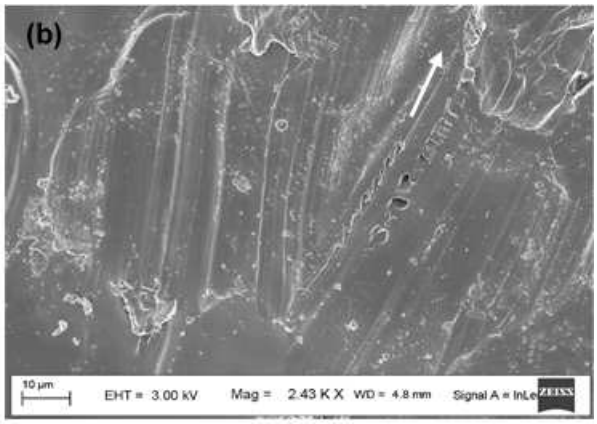

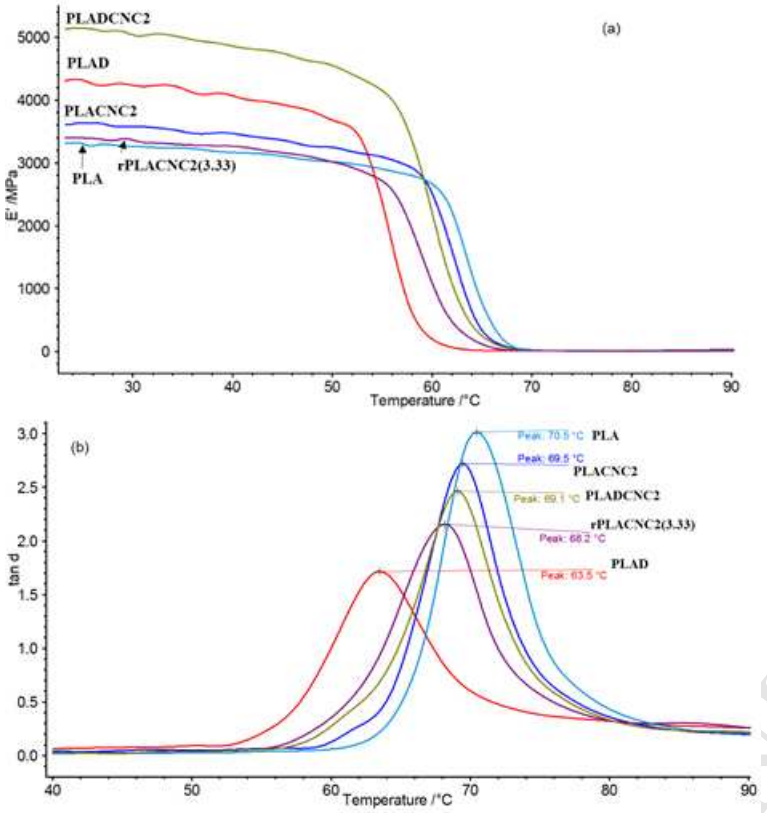

Highlights

- PLA chains grafted onto CNC surface (PLA-*g*-CNC) through C-C bond formation in presence of dicumyl peroxide radical.
- PLA-*g*-CNC nanocomposite films were found to be thermally stable and could be recycled.
- PLA-*g*-CNC films shows uniform dispersion of CNC due to the efficient grafting, results in improvement in tensile strength.
- Crystalline behavior and elastic properties of resulting composites improved with increase in the CNC loadings.